2004-12-08

Atomic Force Microscope Conductivity Measurements of Single Ferritin Molecules

Degao Xu
Brigham Young University - Provo

ATOMIC FORCE MICROSCOPE CONDUCTIVITY MEASUREMENTS OF SINGLE FERRITIN MOLECULES

by

Degao Xu

A dissertation submitted to the faculty of

Brigham Young University

in partial fulfillment of the requirements for the degree of

Doctor of Philosophy

Department of Physics and Astronomy

Brigham Young University

October 2004

BRIGHAM YOUNG UNIVERSITY

GRADUATE COMMITTEE APPROVAL

of a dissertation submitted by

Degao Xu

This dissertation has been read by each member of the following graduate committee and by majority vote has been found to be satisfactory.

Date	Robert C. Davis, Chair
Date	Bret C. Hess
Date	William E. Evenson
Date	David D. Allred
Date	Richard H. Selfrige

BRIGHAM YOUNG UNIVERSITY

As chair of the candidate's graduate committee, I have read the dissertation of Degao Xu in its final form and have found that (1) its format, citations, and bibliographical style are consistent and acceptable and fulfill university and department style requirements; (2) its illustrative materials including figures, tables, and charts are in place; and (3) the final manuscript is satisfactory to the graduate committee and is ready for submission to the university library.

_____
Date

_____
Robert C. Davis
Chair, Graduate Committee

Accepted for the Department

_____
Ross L. Spencer
Graduate Coordinator

Accepted for the College

_____
Earl M. Woolley
Dean, College of Physical and Mathematical Sciences

ABSTRACT

ATOMIC FORCE MICROSCOPE CONDUCTIVITY

MEASUREMENTS OF SINGLE FERRITIN MOLECULES

Degao Xu

Department of Physics and Astronomy

Doctor of Philosophy

Conductive Atomic Force Microscope (c-AFM) was used to measure the conductivity of single horse spleen ferritin (HoSF) and azotobacter vinelandii bacterial ferritin (AvBF) molecules deposited on flat gold surfaces. A 500μm diameter gold ball was also used as a contact probe to measure the conductivity of a thin film of ferritin molecules. The average current measured for holo HoSF was 13 and 5 times larger than that measured for apo HoSF as measured by c-AFM at 1V and gold ball at 2V and respectively, which indicates that the core of ferritin is more conductive than the protein shell and that conduction through the shell is likely the main factor limiting electron transfer. With 1 volt applied, the average electrical currents through single holo HoSF and single apo HoSF molecules were 2.6 pA and 0.19 pA respectively. Measurements on holo AvBF showed it was more than 10 times as conductive as holo HoSF, indicating that the protein shell of AvBF is more conductive than that of HoSF. The increased conductivity of AvBF is attributed to heme groups in the protein shell.

ACKNOWLEDGMENTS

I would like to express my gratitude for the help I received from so many teachers and students at BYU. Foremost, I would like to thank my advisor, Dr. Robert Davis; he invested so much time on this project. I really appreciate his help, patience, discussions, and encouragement.

All the ferritin solutions were provided by Dr. Gary Watt and his student Bo Zhang. The discussions with them about the structure and properties of ferritin gave me a great help for this research project. I would like to thank Dr. John Harb, the group leader of the nano-battery project. He not only directed the contact with the funding agency NASA to support this project, but he also gave me some helpful suggestions, discussions, and encouragement.

I appreciate Dr. James Lewis and Dr. Bret Hess's help for the discussion about this project. I'm also grateful for the help from Diann Soreson and Nan Ellen Ah You and Scott Daniel. I would like to thank Tim Miller, Jed Whittaker, Brad Strongin, Dan Allan, Brent Waccaser, and other students who gave me some help for my research work.

I especially want to express my gratitude to Dr. Harold Stokes, who gave me a great deal of help for my early graduate study at BYU. By his recommendation, I had a summer research internship at Los Alamos National Lab, which gave me an invaluable research experience.

Finally, I would like to thank my wife, Hongguang Zhao, and my son, Zhoyue Xu. Without their support and patience, I couldn't finish my research project.

Contents

List of Figures

Chapter 1

Introduction

Ferritin, an iron storage protein, is found in almost all biological systems[1][2]. Iron in the soluble form Fe(II) in the living environment is essential for its role in oxidation-reduction reactions and certain types of catalysis. Excessive Fe(II) can be very toxic and damage cells because of its propensity to form oxygen radicals. Nature has evolved to meet this iron problem by a set of iron storage proteins that store iron and prevent it from damaging other molecules, yet allow it to be released when needed. Each ferritin molecule has a spherical protein shell which can store 2000 to 4500 irons as Fe(III).

1.1 Structure of Ferritin

Ferritin is a large protein with a diameter ~12nm. The protein coat of ferritin, apoferritin, consists of 24 protein subunits arranged in 432 symmetry to give a hollow shell with a ~8nm diameter cavity. The subunits were designated H(eavy) and L(ight)[3], which differ in size, amino acid composition, surface charge, mobility, and immunoreactivity. Ferritin molecules isolated from vertebrates are composed of H and L subunits, whereas those from plants and bacteria contain only H subunits. H-chains catalyze the oxidation of the toxic Fe(II) atoms into Fe(III) atoms and L-chains help for the core formation[1][2]. The molecular weight of ferritin is 474,000g/mol.

Proteins contain 20 different amino acids[4]. All amino acids have the format NH_3^+-CHR-COO^-, where R indicates as a side chain. Each amino acid has an amino group (NH_3^+), a carboxyl group (COO^-), a hydrogen atom (H), and a side chain (R). Appendix 1 lists all twenty amino acids, including their names, abbreviations, and linear structures. The amino acids join together in proteins via peptide bonds. One molecule of water forms as a by-product after two amino acids combine to form a bipeptide. This gives rise of the name polypeptide for a chain of amino acids. A protein can be composed of one or more polypeptides. A polypeptide chain has polarity. One end of the chain has a free amino group. It is called amino terminus, or N-terminus. The other end has a free carboxyl group. It is called carboxyl terminus, or C-terminus. N-terminus is positively charged and C-terminus is negatively charged. The linear order of amino acids constitutes a protein's primary structure. The way these amino acids interact with their neighbors gives a protein's secondary structure. The alpha helix is a common form of secondary structure. It results from the hydrogen bonding among near-neighbor amino acids. In alpha helix structure all R groups of the amino acids extend to the outside. The helix makes a complete turn every 3.6 amino acids. The helix is right-handed; it twists in a clockwise direction.

Horse spleen ferritin (HoSF) is widely studied because it is composed (85%) of identical subunits and because high-resolution X-ray crystallography makes it possible to determine locations of all the amino acids[5,6]. Each subunit contains 174 amino acids [7]. As shown by Figure 1-1, each subunit consists of four long alpha-helices(A, B, C and D), a fifth short alpha-helix(E) and a long loop(L), which connects two pairs of alpha-helices(A and C, B and D).

Channels (small holes through which certain ions or molecules can travel) in the sphere are formed at the intersections of three or four peptide subunits. These channels are critical to ferritin's ability to release iron in a controlled fashion[9]. Two types of channels exist in ferritin. Four-fold channels occur at the intersection of four peptide subunits. Three-fold channels occur at the intersection of three peptide subunits. These two types of channels have different chemical properties, and hence are believed to perform different functions. Four-fold channels are non-polar and hydrophobic. The functions of four-fold channels may include exchanging oxygen and anions into the ferritin cavity. Three-fold channels are polar and hydrophilic. These channels are narrow, restricting access to small molecules and metal ions. The functions of three channels include the initial binding and possible oxidation of ferrous ion[10, 11].

Azotobacter vinelandii baterial ferritin (AvBF)[12] is another ferritin used for this project. The structure of AvBF is quite similar to the structure of HoSF. The notable differences include[13, 14]: 85% of the HoSF subunits are L-chains while all of the AvBF subunits are H-chains; AvBF has 12 heme groups while HoSF has no heme groups; the core of HoSF is mineral ferrihydrite with some phosphate (Fe:P =10:1) while the core of AvBF is amorphous phospho-hydroxy iron mineral with more phosphate (Fe:P=1:1). Each heme is located in the middle of two protein subunits along the two-fold axis[2]. It starts from the ferritin core and extends toward the outside surface of the ferritin protein shell.

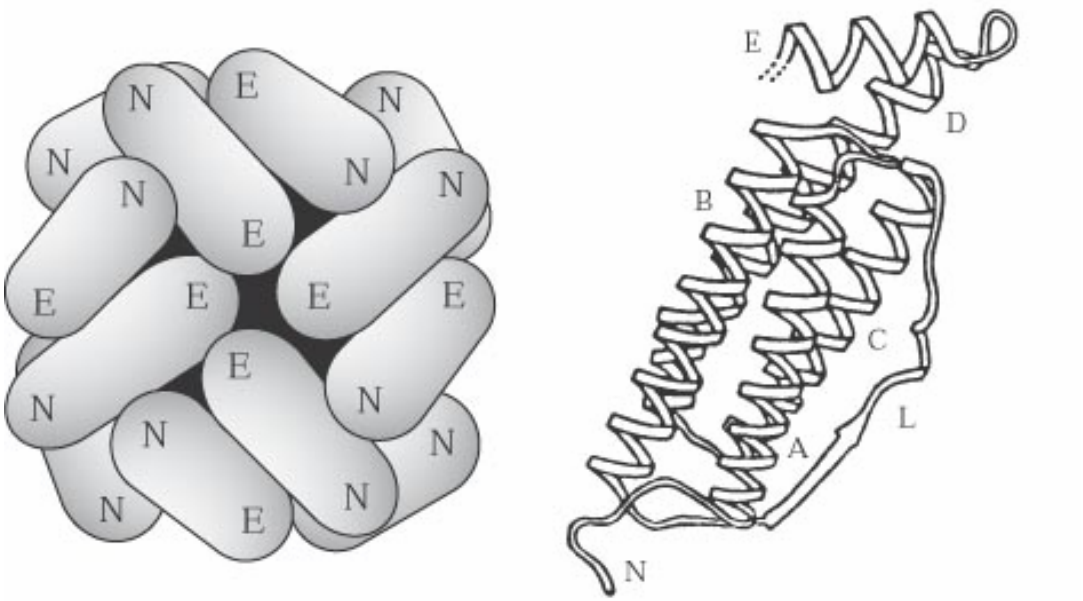

Figure 1-1. The structure of Ferritin. Ferritin is composed of 24 subunits. Each subunit is represented by a sausage-shaped building brick. The N-terminal region of the polypeptide chain lies close to the end labeled N; the E helix residues lie close to the end labeled E. Ribbon diagram of alpha carbon backbone of a horse spleen ferritin is also shown. The four long alpha helixes A, B, C, and D are comprised of residue 10-39, 45-72, 92-120, and 124-155 respectively; helix E contains residue 160-169. L, a loop, connected B and C, contains residues 73-91[2,8]. Reprinted with the permission of the original authors[8].

1.2 The Core of Horse Spleen Ferritin

Ferritin with an empty core is called apoferritin. In nature, ferritin has a iron core (called holoferritin), with a structure quite similar to the mineral ferrihydrite[15, 16, 17, 18]. The soluble Fe(II) enters the protein shell and goes through the following chemical processes to form the iron core[19]:

$$2Fe^{2+} + O_2 + 6H_2O \rightarrow 2Fe(OH)_3 + H_2O_2 + 4H^+$$

$$4Fe^{2+} + O_2 + 10H_2O \rightarrow 4Fe(OH)_3 + 8H^+$$

When ferritin releases iron, electrons are transferred through the protein shell to reduce the Fe(III) in the mineral lattice to Fe(II), thereby to render the iron soluble so that it can be released from ferritin.

It is difficult to characterize the exact structure of ferrihydrite[20]. The common designations includes amorphous iron hydroxide, colloidal ferric hydroxide, $Fe(OH)_3$, etc. The identification techniques for ferrihydrite includes X-ray diffraction, infrared spectrum, Mossbauer spectroscopy, differential dissolution. Ferrihydrite is generally classified according to the number of X-ray diffraction lines: 2-line ferrihydrite and 6-line ferrihydrite[21, 22, 23]. 2-line ferrihydrite exhibits little crystallinity while 6-line ferrihydrite is well crystallized. The widely reported nominal formula of ferrihydrite is $5Fe_2O_3 \bullet 9H_2O$. The contemporary models for ferrihydrite are not decisive. The general agreement is that ferrihydrite is not amorphous and it at least has a low degree of crystallinity detectable by X-ray diffraction. The core of ferrihydrite particles consists of irons in octahedral coordination whereas the surface

has most irons in tetrahedral coordination. The coordination-unsaturated surface may account for the high adsorptive capacity of ferrihydrite.

1.3 The Study of Ferritin and Its Applications

As a nanoscale biologically derived material ferritin has been used in a wide range of studies due to its magnetic[24-28], electrochemical[29,30], and directed assembly properties[31,32]. Ferritin has been used to generate other nanostuctured materials both as a catalyst for carbon nanotube growth[33-37], and as a template for the synthesis of magnetic[38-41], conducting[42], and semiconductor nanocrystals[43]. The structural stability, assembly properties, and ability to synthesize a wide variety of cores in ferritin make it a promising component for a diverse array of nanoengineered materials.

We are currently exploring the use of ferritin as a building material for nanoscale batteries. These batteries are based on the redox potential[44] when the ferritin core undergoes an electrochemical reduction reaction[45]. The electrical conductivity of the protein shell is critical to the performance of ferritin-based batteries and will play a significant role in many other ferritin applications.

1.4 The Importance of Conductivity Measurements of Ferritins

Previous electrochemical and chemical and studies on ferritin indicate that the protein shell may act as an electron conductor[29,30,46]. For electrochemical ferritin studies, adsorption of the ferritin to a conductive surface is needed. Ferritin adsorption on gold surfaces has been characterized by various surface and microscopic methods

including Atomic Force Microscopy (AFM)[32]. Electron transfer to and from the mineral core of ferritin absorbed at bare gold electrodes has been studied in phosphate buffer by cyclic voltammetry[29,30]. Ferritin adsorbs at fairly negatively potentials and exhibits reasonably well-defined current-potential curves.

These studies point toward electron conductivity through the ferritin protein shell; however, no direct electron conductivity measurements on ferritin have been reported. The current contributed by each ferritin molecule is also not directly measured by these previous bulk measurements. For nanoscale battery applications, the electron transfer rate through the ferritin is a critically important parameter; it will affect the internal resistance and limit the maximum current. The electrical resistance of the ferritin will also play a critical role in the electronic properties of materials made from assembled ferritins for other applications.

1.5 Review of Conductivity Measurements of Single Molecules and Nanoparticles

Electrical conductivity measurements of single molecules and nanoparticles are usually based on two nanoscale electrodes or AFM techniques. Two nanoscale electrodes may be made by electron-beam lithography and electromigration [47-49]. Molecules or nanoparticles were deposited around the gap area. There may be none, one or more molecules (or nanopaticles) contributing to the measured conductivity. In order to determine if the measured conductivity is from a single molecule (or nanoparticle), the experiments were usually performed at low temperature so that the characteristic I-V curves (due to Coulomb blockade) from a single molecule (or

nanoparticle) could be observed. At room temperature, the experiments were repeated many (thousands) times until the conductance histogram showed peaks at integer multiple of a fundamental conductance, which was used to identify the conductance of a single molecule[50].

Other conductivity measurements of single molecules and nanoparticles are based on conductive AFM[51, 52, 53]. Molecules or nanoparticles were deposited on a flat conductive surface. A conductive AFM tip was used to image molecules (or nanoparticles) by contact mode AFM. The current-voltage characteristic curves were measured by positioning the conductive AFM tip on the top of molecules (or nanoparticles). Conductive AFM was widely used to measure the local conductivity of thin molecule layer (or monolayer) by positioning the conductive tip on the top of the thin film layer. Some of these experiments showed that current-voltage curves could be quantized as integer multiple of one fundamental curve, which was used to identify the I-V curves of a single molecule.

For our AFM I-V measurements of single ferritin molecules, tapping mode AFM was used to image ferritin molecules. Then a script program was used to bring the AFM tip into contact with an individual ferritin molecule to perform the electrical measurements.

1.6 Brief Review of This Project

First, flat gold surfaces were fabricated by using the mica surfaces so that ferritin molecules absorbed onto such gold surfaces could be imaged clearly by the tapping mode AFM. Then, electrical conductivity measurements on single horse

spleen ferritin (HoSF) molecules on gold surfaces were performed by conductive AFM. Conductivity measurements on monolayer films of ferritins were also performed for comparison with the single molecule measurements. Conductivity measurements were also performed on AvBF. Finally, Fowler-Nordhein tunneling model was used to fit the the measured I-V curves so that we could get an expression of the barrier height between ferritin protein shell and gold surface.

1.7 Organization of the Thesis

Chapter 2 provides the detailed experimental procedures used for ferritin conductivity measurements, including: AFM, conductive AFM, ferritin-Au sample preparation, and experimental methods for conductivity measurements. Chapter 3 presents the experimental results of conductivity measurements on horse spleen ferritin. Chapter 4 gives the experimental results of conductivity measurements on azotobacter vinelandii bacterial ferritin. Chapter 5 analyses the conductivity results from Chapter 3 and Chapter 4. Chapter 6 provides conclusions on this project and some suggestions for the future work.

Chapter 2

Conductivity Experimental Methods

2.1 Atomic Force Microscope (AFM)

An atomic force microscope (Digital Instrument Dimension 3100) was frequently used for this project. The AFM system is comprised of two main components: the scanner and the AFM detecting system as shown in Figure 2-1. There is a piezoelectric transducer in the scanner. The piezo element can drive the tip or the sample in the X, Y and Z direction. The AFM tip is positioned at the end of a micro-fabricated cantilever. The AFM detecting system uses a laser beam which is reflected from the cantilever into a mirror and finally into a pair of photodiodes. So the behavior of the tip while scanning on the sample surface is monitored by the photodiodes. There were three modes which were used for this project: contact mode, taping mode and force mode.

In contact mode (or static mode) AFM, the tip is in mechanical contact with the sample surface at a set applied force. The precise applied force can be evaluated with force mode AFM. Figure 2-1 shows how contact mode AFM works. While the tip is scanning on the sample surface, the feedback loop of the detecting system adjusts the height of the tip so that the deflected laser from the cantilever maintains a predetermined vertical position on the photodiodes.

Contact mode AFM is not effective for imaging ferritin molecules physisorbed on gold surfaces. When ferritin molecules are imaged on gold surfaces, even at the

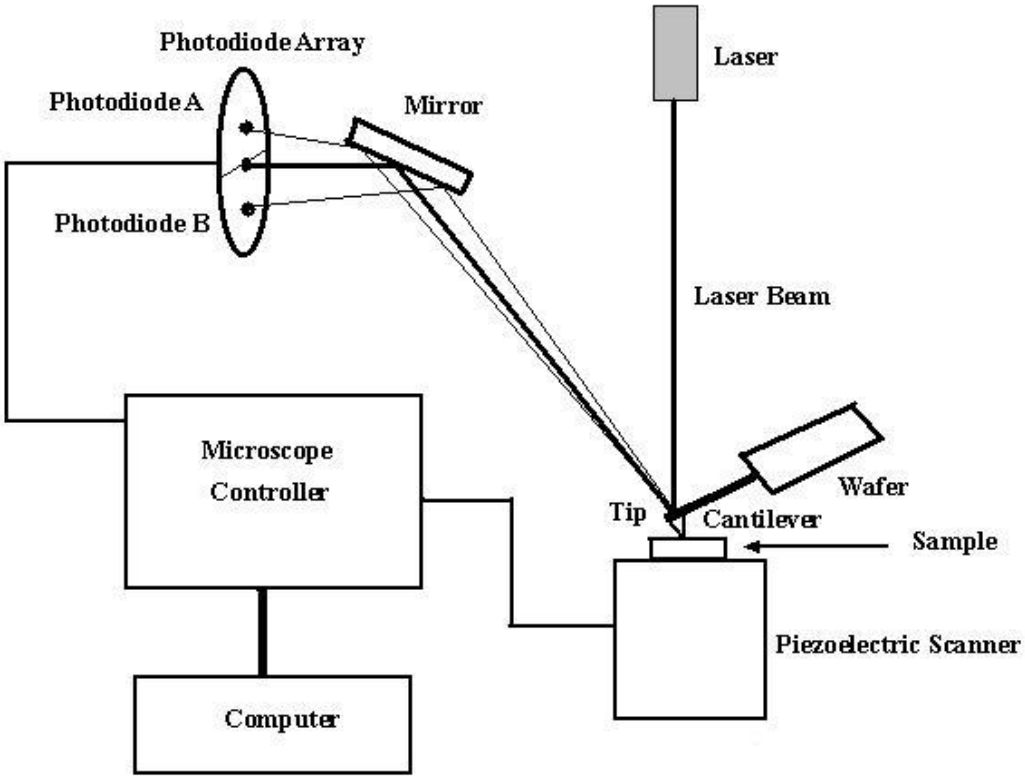

Figure 2-1. Contact mode AFM. The feedback loop maintains a constant cantilever deflection while the tip is scanning on the sample surface.

lightest imaging force available, the ferritin molecules are still moved around on the gold surface(shown in Figure 2-2). After several images, almost all the ferritin molecules are pushed out of the scanning area. A tapping mode AFM image (Figure 2-3) shows the final distribution of ferritin molecules in the nearby area. In this project, contact mode AFM was used primarily to test the conductivity of AFM tips on clean gold surfaces.

In the tapping mode (or dynamic mode) AFM, the tip is not in continuous contact with the sample surface. Instead the cantilever is oscillated at its resonance frequency above the sample surface, causing the tip to tap the surface as it oscillates. The RMS amplitude of the signal from the photodiode is compared to a setpoint amplitude. The feedback loop keeps the vibrating cantilever at a constant amplitude by adjusting the tip height while the tip is scanning on the sample. The main advantage is that tapping mode AFM can image weakly bound molecules, like ferritin, clearly. Tapping mode was the mode used for all further ferritin molecule imaging. Appendix 2 gives some tapping mode AFM images of ferritin molecules on flat gold surfaces.

In the force mode AFM, force-distance curves are obtained by extending the tip to the surface to make contact and then increase the force between the tip and surface followed by retracting the tip from the surface. If the spring constant of the cantilever is known, this curve may be used to determine the contact force. In this project, we use this curve to determine the contact force between the tip and ferritin molecules during conductivity measurements. Figure 2-4 shows a force-distance curve between the tip and horse spleen holoferritin on a flat gold surface.

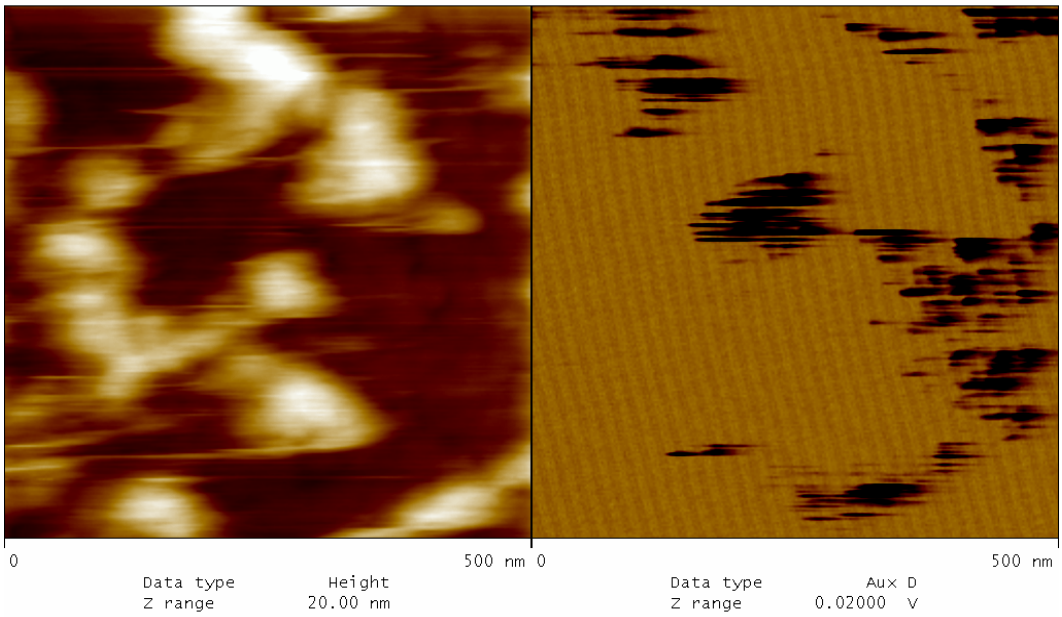

(a) (b)

Figure 2-2. (a) Image of ferritin molecules on a flat gold surface using contact mode AFM. (b) Current image of the same area. The conductive AFM was applied with a constant voltage 0.5V while the tip was scanned to image ferritin molecules.

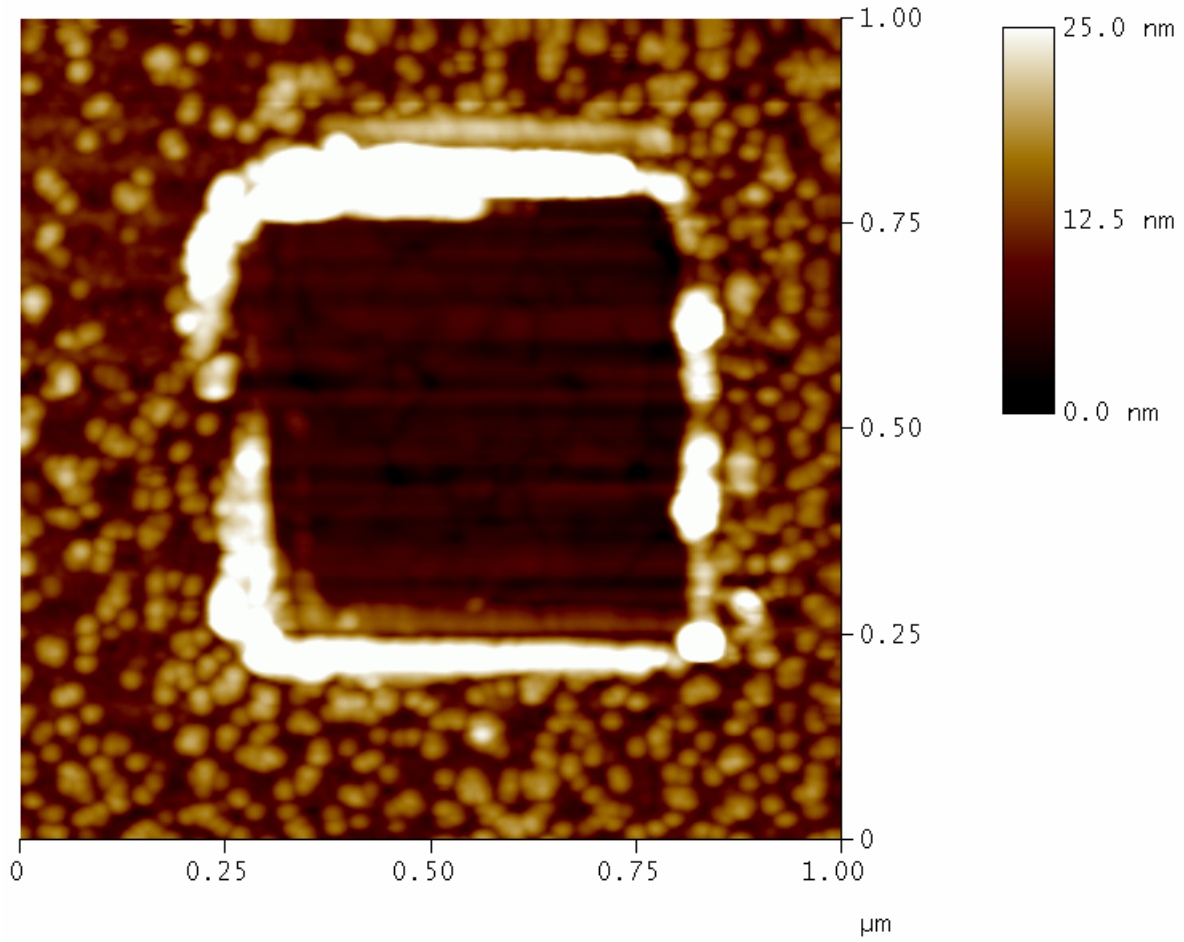

Figure 2-3. Tapping mode AFM image of ferritin molecules in the area near to the square scanned by the contact mode AFM.

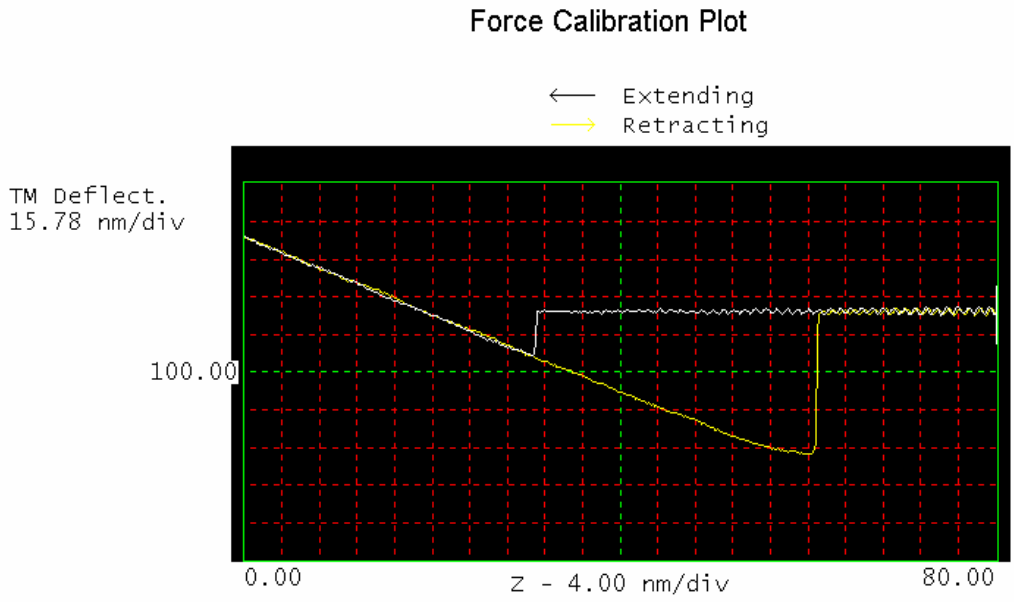

Figure 2-4. The force-distance curve between the tip (NCS12-E) and horse spleen holoferritin on a flat gold surface.

2.2 Conductive AFM Tip

The probes we used for the I-V measurements were purchased from MikroMasch (www.spmtips.com). Each chip has 6 cantilevers. Figure 2-5 shows the layout of the 6 cantilevers on a chip. For our conductivity measurements, we only used soft tips D, E and F. Their typical spring constants are 0.35, 0.30 and 0.65nN/m respectively.

A Cr-Au coating is formed on the tips as a 20-nm gold film on a 20-nm chrome sublayer, which increases adhesion of gold. This Cr-Au coating is chemically inert. The resulting radius of curvature of the tip is less than 50 nm. The full tip cone angle is 30° and tip height is about 15~20 μm. In our experiments, we only used cantilever D, E and F. The tips under these cantilevers were used for both imaging ferritin molecules by taping mode AFM and for conductivity AFM measurements of ferritin molecules.

2.3 Atomically Flat Gold Surface

A template-stripped method [54] was used to prepare the flat conductive gold surfaces needed to image ferritin clearly by tapping mode AFM and to perform conductivity measurements. Briefly, V-1 grade mica (Structure Probe, Inc. / SPI Supplies, West Chester, PA) was cleaved with a sharp scalpel knife. Gold (99.99%) was then thermally evaporated onto the freshly cleaved mica at a pressure of ~4 $\times 10^{-6}$ torr. The deposition rate was kept at ~1Å/sec for the first minute and then increased to 10Å/sec to yield a 200nm thick gold film. A drop of low viscosity epoxy glue (EPO-TEK 377) was applied to the gold surfaces and the samples were glued to

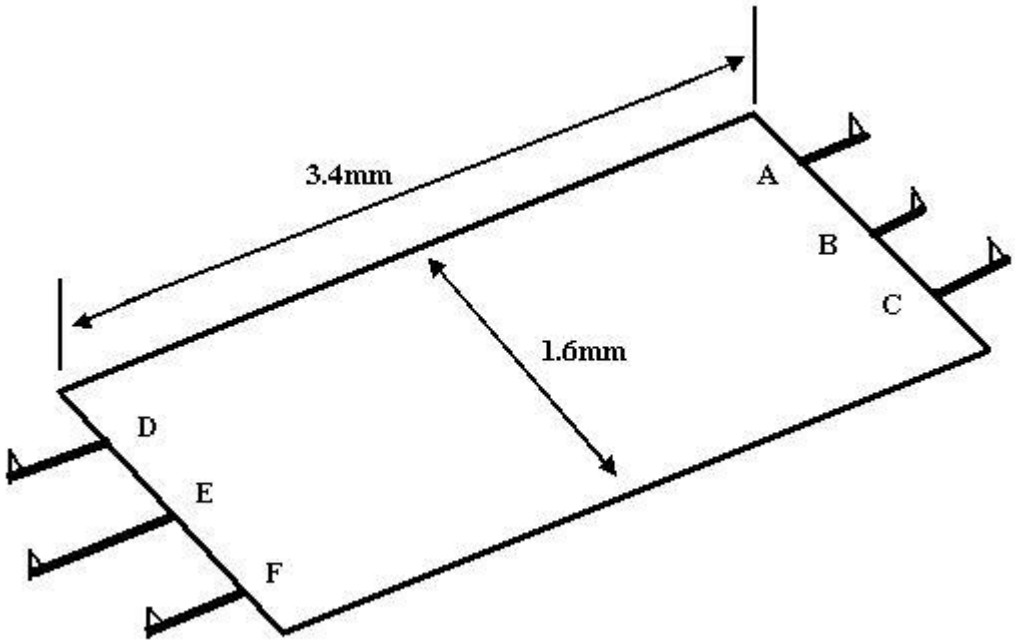

Figure 2-5. The layout of the 6 cantilevers(A, B, C, D, E, F) on a NCS12 chip. The thickness of the chip is 0.4 mm.

pieces of silicon wafer or to glass slides. The samples were then baked in an oven at 150 ºC for 1~2 hours. Finally, the Au film was released from the mica by immersion in tetrahydrofuran (THF) for 5 minutes. The roughness of the resulting gold surface was less than 0.5nm locally, which is an ideal surface for visualization of ~10nm ferritin molecules by AFM. Figure 2-6 shows the first four steps to make flat gold surfaces. The improvement of the gold surface flatness is shown in Figure 2-7. The two tapping mode AFM images use the same height scale.

2.4 Deposition of Ferritins on Flat Gold Surface

Horse spleen ferritin (91mg/ml) in 0.15M sodium chloride was purchased from Sigma. Ferritin solutions were made by diluting the stock solution to the desired concentration with 0.05M phosphate buffer, pH 7.4, containing 0.05M NaCl,. Several drops of ferritin solution were applied to the flat gold surface, allowing a self-assembled layer of ferritin molecules to form on the surface. The sample was then rinsed with Milli-Q water for one minute. Finally, the surface was dried with nitrogen. Appendix 2 gives some tapping mode AFM images of ferritin molecules on flat gold surfaces.

2.5 Experimental Determination of Ferritin Conductivity

2.5.1 Single Molecule AFM Conductivity Measurements

Au coated AFM probe tips (20nm Au overall coating with 20nm Cr sublayer) were used for conductivity measurements. The experiment setup is shown on Figure

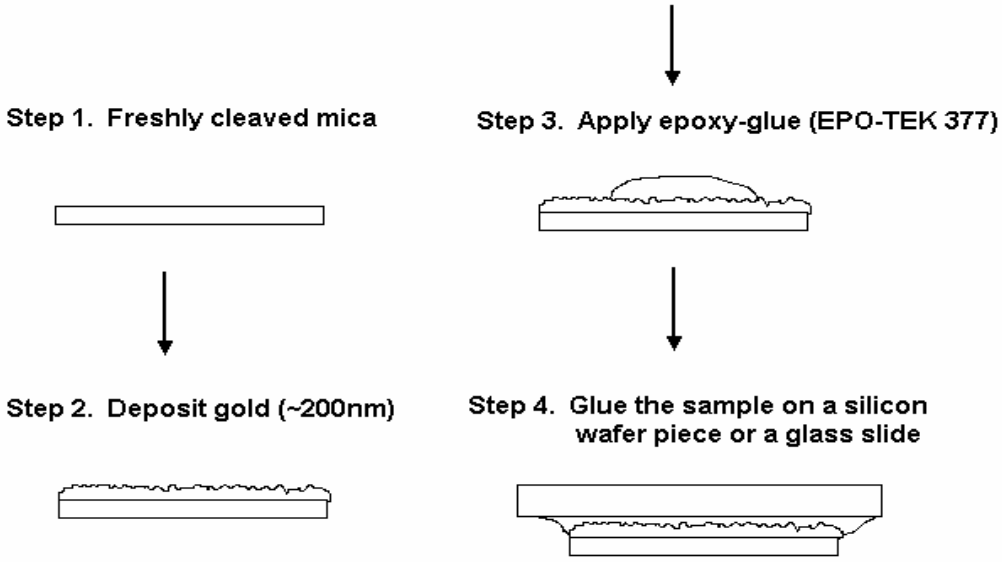

Figure 2-6**.** The first four steps of the template-stripped method to make an atomically flat surface. Finally (Step 5), the mica is stripped away by the chemical solvent tetrahydrofuran (THF).

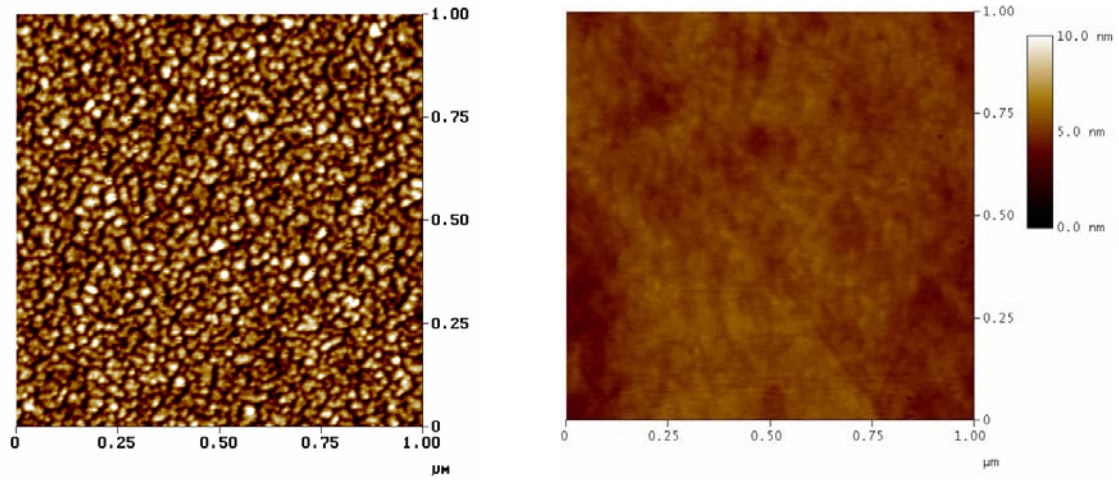

(a) (b)

Figure 2-7. Tapping mode AFM images of gold surfaces. (a) The tapping mode AFM image of a gold surface deposited by conventional thermal evaporation. (b) The tapping mode AFM image of a gold surface prepared by the template stripped method. The two images are on the same vertical scale.

2-8. Ferritin molecules were deposited on a flat gold surface with very low coverage (<100 ferritins /μm^2) and a Dimension 3100 AFM (Digital Instruments) in tapping mode was used to find a candidate ferritin molecule for the current-Voltage (I-V) measurements. Its height was 9~10nm. The target molecule was then imaged in a 100nm × 100nm field of view. The AFM X and Y offsets were adjusted repeatedly to center the ferritin in the field of view until the drift stabilized; this stabilization usually took ~ 30 minutes. A Nanoscript (Nanoscope III version 4.43r8) program (shown in Appendix 3) was then run, which lowered the AFM tip into contact with the top of the ferritin molecule. Then the Nanoscript program triggered a separate computer running a LabVIEW (National Instruments, version 6.1) program (also shown in Appendix 3) to perform an I-V measurement on the molecule with the tip voltage scanning from negative to positive. A current amplifier (DL Instruments Model 1211) was used to amplify the current. The conductive AFM tip was gradually lowered by the Nacoscript program until stable I-V curves were obtained.

2.5.2 Gold Ball Conductivity Measurements

To complement the single molecule measurements, a spherical gold probe (Figure 2-9) was used to perform I-V measurements on a ~3 μm^2 area containing thousands of particles. To make the probe, the end of a 100 μm diameter gold wire was heated in a high temperature flame and then cooled to yield a 500 μm diameter sphere at the end of the wire. Figure 2-10 shows SEM and AFM images of the gold probes. Tapping mode AFM images showed that the surface roughness of the gold probe was less than 1nm.

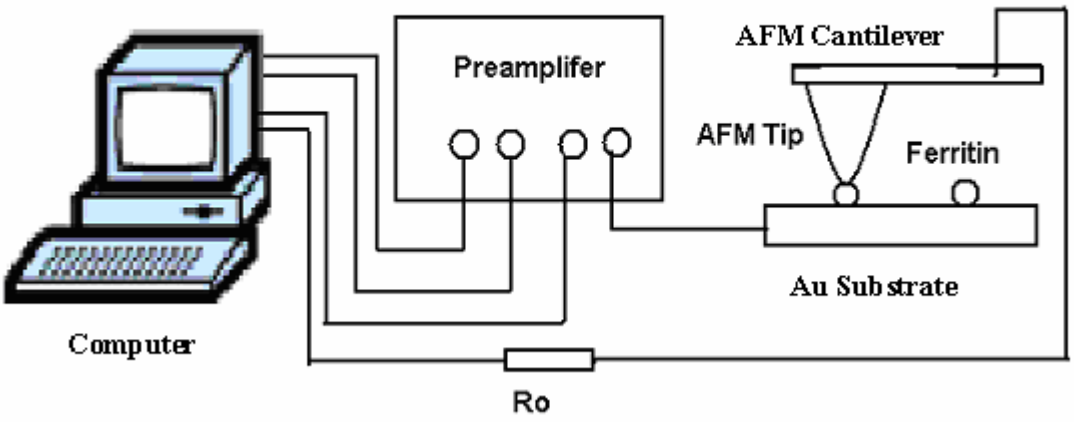

Figure 2-8. The experiment setup for I-V measurements on a single ferritin molecule. R_0 (~$6.7\times10^8\ \Omega$) is used to limit the current. For AFM measurements a low surface density of ferritins (<100//μm^2) was used.

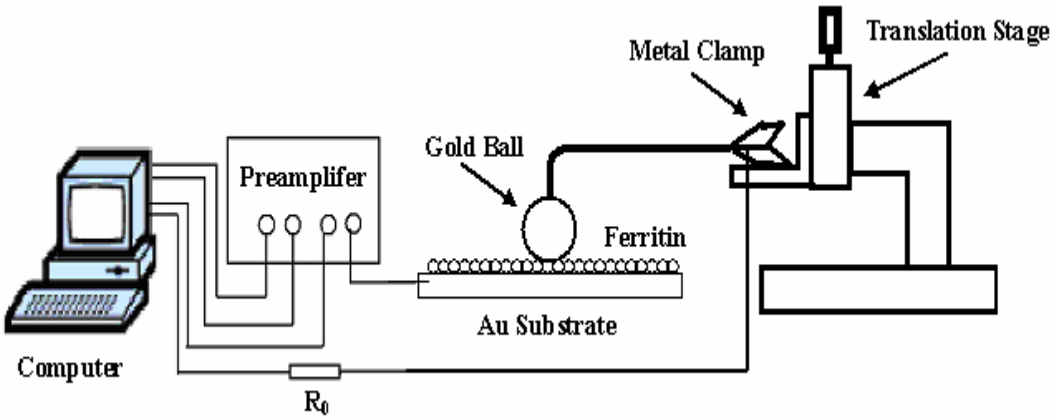

Figure 2-9. The experiment setup for I-V measurements on a film of ferritin molecules by using a gold ball. R_0 (~$2.0\times10^7\ \Omega$) is used to limit the current. A gold ball with a diameter of 500um is used as a current probe for a ferritin film. The gold ball is held with a clamp. The height of the gold ball was adjusted using the translation stage micrometer. The surface density of ferritins for these measurement was ~1100/μm^2.

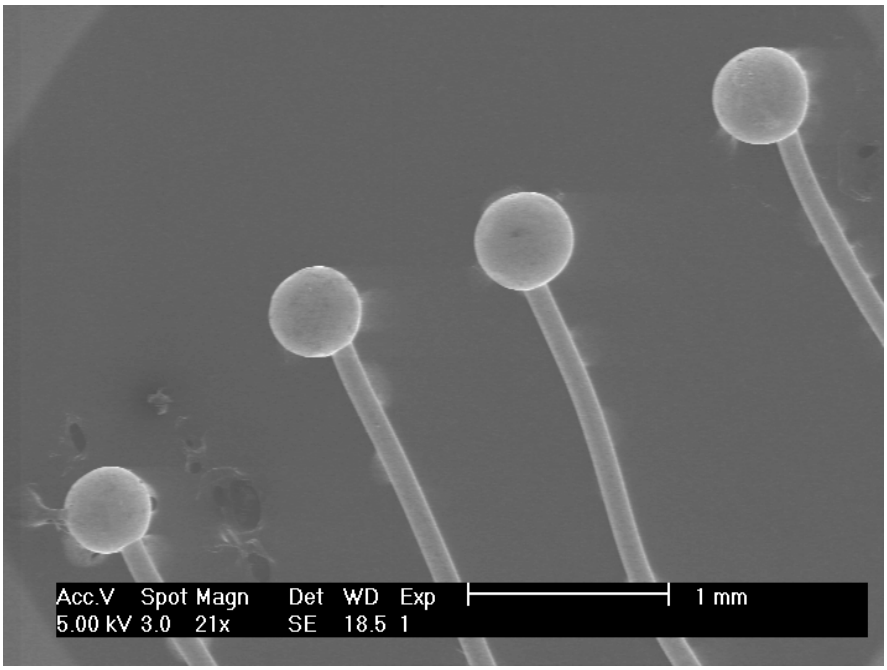

(a)

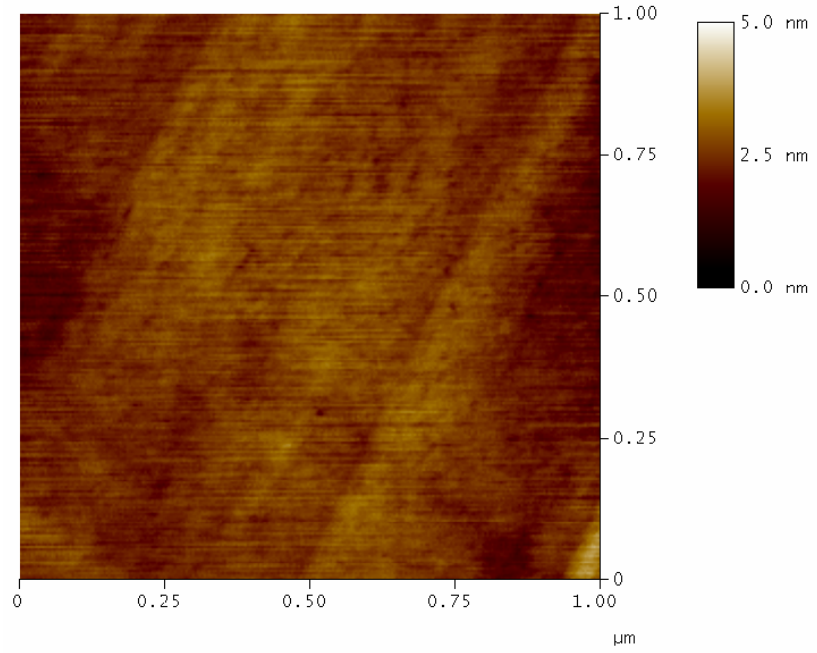

(b)

Figure 2-10. SEM and AFM images of the gold ball surfaces. (a) SEM image of four gold balls formed on the ends of gold wire with diameter 0.1 millimeters by burning these ends in a high temperature flame. (b) Tapping mode AFM image of the surface of a gold ball. The flatness of the surface is less than 1nm, which is much smaller than the height of ferritin molecules(~10nm).

The gold ball was used to make film contuctance measurements similar to the single molecule AFM conductance measurements. A micrometer was used to gently lower the probe onto the ferritin-coated surface. The contact force between the spherical probe and the flat gold surface was gradually increased until stable I-V curves were obtained. The contact force between the gold ball and the sample was calculated from the gold wire physical dimensions and the bending of the gold cantilever beam (wire) by the following equation[55]:

$$F = k\Delta x = \frac{3EI}{L^3}\Delta x$$

where Δx is the bending distance of the free end, E is the Young's modulus of elasticity, L is the length of the cantilever beam, and I is the moment of inertia. The cantilever beam has a circular cross section with radius r (or diameter D) giving a moment of inertia:

$$I = \frac{\pi r^4}{4} = \frac{\pi D^4}{64}.$$

The Young's modulus of elasticity of gold is 79GPa.

2.5.3 The Conductivity of the AFM Tip and the Contact Resistance between the Tip and Flat Gold Surfaces

Since gold is such a soft metal, the Au coated conductive AFM tip can be damaged and lose its conductivity very quickly if the tip is used inappropriately. We found that that the AFM tip lost its conductivity when the tip was in contact with the gold surface for one minute at current of 20nA. We also saw evidence of gold transfer from the tip to the substrate gold surface at 20nA (Figure 2-11 (a)); gold dots were deposited on the substrate. In our conductivity experiments, we limited the tip current

to less than 3 nA. In this range, we didn't see gold transfer from the tip to the gold substrate. Another factor to consider is the contact force between the tip and the substrate surface. When the tip was scanned at an applied force larger than 20 nN with no applied voltage, the tip also lost its conductivity quickly.

To perform conductivity measurements, we adjusted the target ferritin molecule to the center of the view area and then ran a Nanoscript program intended to position the tip at the center of the view area. The gold transfer dots created at 20nA were used to verify that the script program would position the AFM tip in the center of the image. The alignment of the dots with the image center showed that the tip is sufficiently well centered for ferritin conductivity measurements

When a Au-coated tip was used to get a current image of a flat gold surface, we found that the contact resistance was quite high if the applied force between the tip and the flat gold surface was less than 6nN. In fact, we saw no current in most areas of the scanned flat gold surface. Only when the applied contact force was ~ 6nN or larger, could a reasonable current image of the gold surface be obtained. In order to reduce the contact resistance and obtained stable I-V measurements, all the I-V measurement of single ferritin molecules were done at a contact force of ~6nN or larger.

Prior to performing the Ferritin I-V measurements, we tested the Au-coated AFM tip conductivity. To test the conductivity, tip current as function of tip depth (or tip position) was measured. Figure 2-12 (a) and Figure 2-12 (b) show the measured tip deflection-depth curve and the corresponding current-depth curve. A constant voltage 0.5V was applied to the tip. The spring constant of the cantilever was 0.65N/m. For a

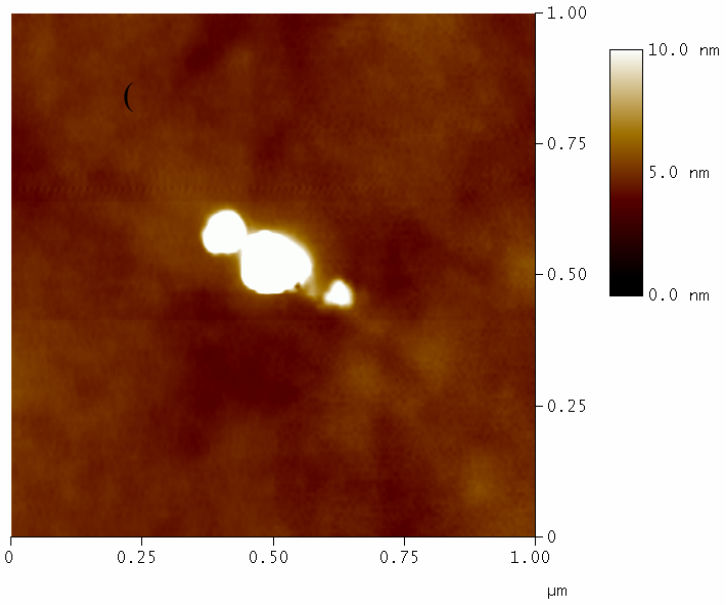

(a)

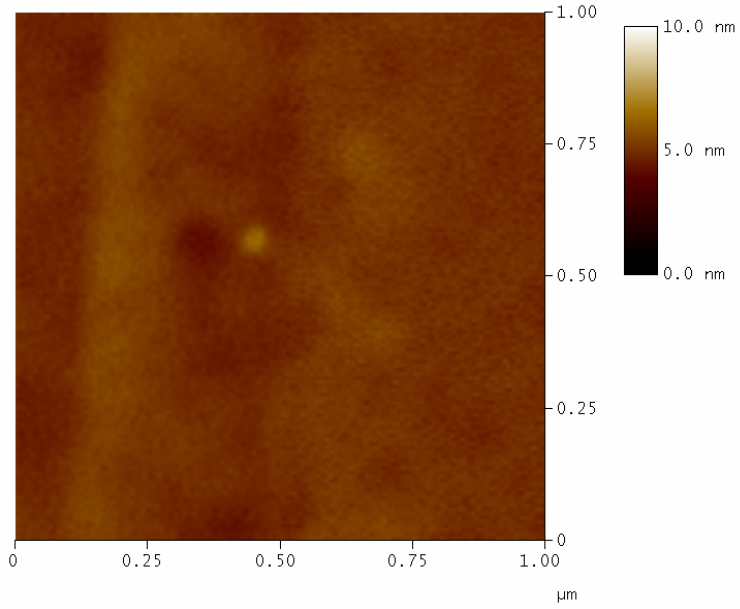

(b)

Figure 2-11. Two taping mode AFM images of the flat gold surfaces. (a) The AFM image of the gold surface after a Au-coated tip with 20nA current positioned at the center of the view area for one minute. The tip transferred some gold onto substrate Au surface. (b) The AFM image of the gold surface after a Au-coated tip with 5nA current positioned at the center of the view area for one minute. There was a small gold dot transferred onto the substrate surface. When the tip current was less than 3nA, no gold transfer from the tip to the surface was observed.

good conductive tip and a clean good surface, the current reached its saturation value when the applied contact force was ~6nN or higher. The conductivity of the tip was also tested using I-V measurements performed with an AFM tip in contact with a clean Au surface. For a good conductive tip and a clean Au surface, the measured I-V curve was a stable straight line as shown in Figure 2-12 (e) and the contact resistance was less than 10 MΩ.

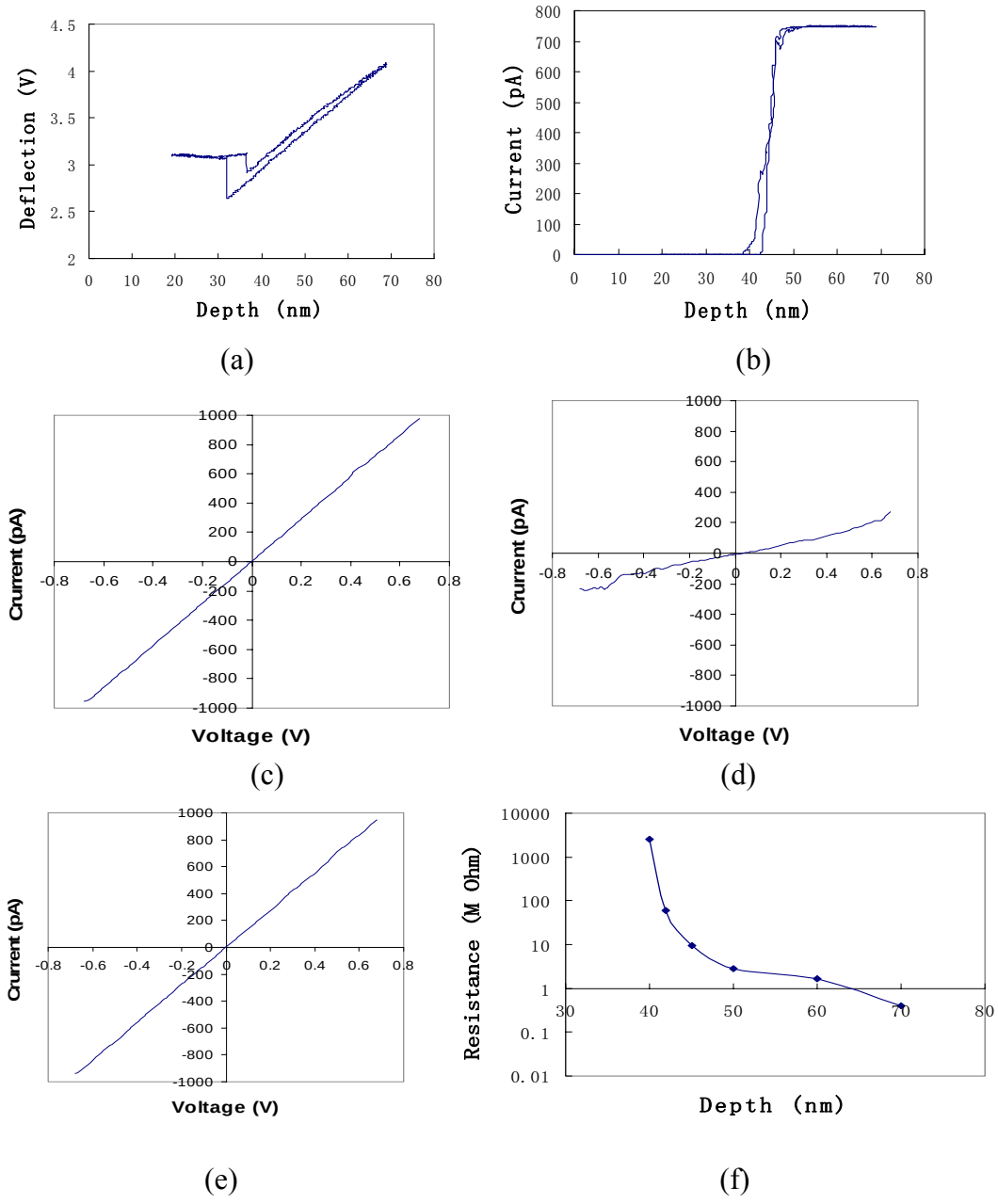

Figure 2-12. The deflection-depth curve and current-depth curve of the tip, and current-voltage curves and resistance-depth curve between a Au-coated tip and a flat gold surface. (a) The deflection-depth curve of a conductive tip with a spring constant 0.65 N/m. (b) The corresponding current-voltage curve of conductive tip while the tip is applied 0.5 volt relative to the gold surface. (c) The current-voltage curve of the resistor R_0(~677MΩ). (d) The current-voltage curve of the contact between the tip and the Au surface with a contact force 2.6nN. The contact resistance was 2.6GΩ. (e) The current-voltage curve of the contact between the tip and the Au surface with a contact force 9.1 nN. The contact resistance was 2.8 MΩ. (f) The contact resistance-depth curve of the contact between the Au-coated tip and the Au surface.

Chapter 3

I-V Measurements of Horse Spleen Ferritin

3.1 The Results of Single HoSF Measurements

Ferritin molecules deposited on the gold surface were imaged by tapping mode AFM as shown in Figure 3-1 for two samples used for single ferritin I-V measurements. These samples were intentionally made with low ferritin densities so that individual molecules could be isolated and identified for the I-V measurements. Individual ferritin molecules were clearly identifiable in the images, although some variation in the height of different molecules was observed. The measured heights of the molecules by AFM was 9.74 ± 0.45nm for holoferritin and 9.24±0.38 nm for apoferritin. These heights are lower that the expected ferritin diameter(~12 nm), this could be due to a slight compression of the molecules or the presence of a thin contamination layer on the surface surrounding the molecule. Single molecule I-V measurements were made on molecules whose height was close to the average molecular height for the sample of interest. The lateral size of the image of a ferritin will is related to the AFM tip size. Appendix 3 gives more detailed discussion between their relationship.

Approximately six thousand I-V measurements were performed on more than 200 single ferritin molecules. Approximately 15 % of the molecules measured showed a current greater than 0.1 pA (our detection limit) and had stable I-V curves when the

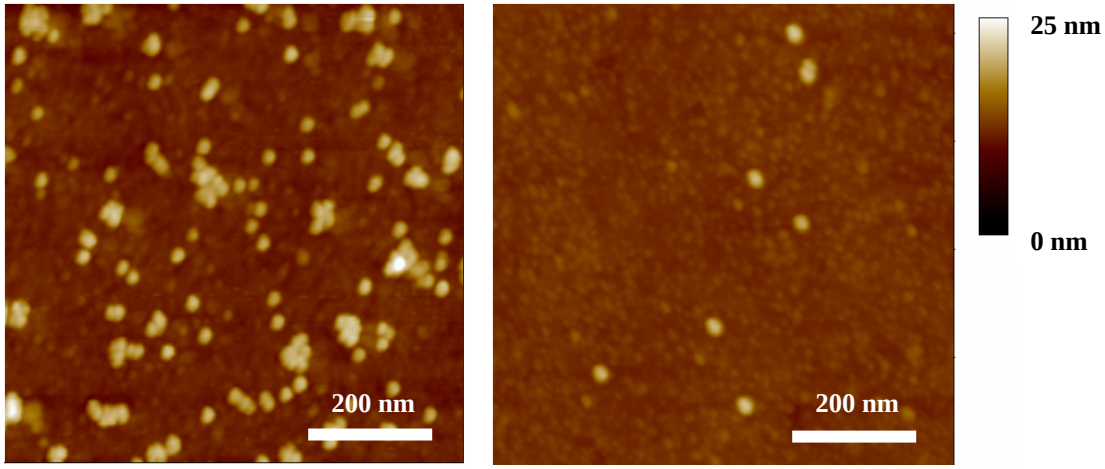

(a) (b)

Figure 3-1. Tapping mode AFM images of apoferritin molecules (a) and holoferritin molecules (b) deposited on a flat gold surface with low ferritin density. The two samples were prepared by applying apoferritin and holoferritin solutions with concentration 0.1mg/ml on flat gold surfaces for 30 seconds and 5 seconds respectively. These two samples were used for single ferritin molecule AFM conductivity measurements.

applied voltage was below 1.5 V. Representative I-V curves on these single ferritin molecules are shown in Figure 3-2 (a). The magnitude of the current observed for the single holoferritin molecules was significantly larger than that observed for single apoferritin molecules at the same applied voltage. The measured I-V curves also showed some asymmetry with a larger current observed for a negative tip voltage than for a positive tip voltage of the same magnitude. Figure 3-2 (b) shows single ferritin conductivity measurements for nine holoferritins and eight apoferritins at an applied voltage of 1V. This figure also gives the standard derivations of the measured current for each molecule. For each molecule, the same I-V measurement was repeated at least 6 times. With 1V applied, the average electrical currents through single holoferritins and single apoferritins were 2.7 ± 1.8 pA and 0.19 ± 0.10 pA respectively. In the range V<0.3 volt, current and the applied voltage roughly have a linear relationship. At V~0 volt, the resistance for holoferritin is ~ $5\times10^{12}\,\Omega$ and the resistance of apoferritins is about ~$1\times10^{13}\,\Omega$.

Stable measurements were obtained at an applied force between 6 and 10nN, and at an applied voltage less than 1.5V. The measured current was unstable when the applied force was less than 6nN. When the magnitude of the applied voltage was > 3 volts or the applied force was > 30nN, the current increased with each successive I-V scan. If the conductivity measurement was interrupted for more than 10 minutes, the ferritin molecule recovered more or less to its initial conductive state. To avoid these instabilities, the data presented and discussed here were all taken at an applied voltage below 1.5V and at an applied force of 6~10 nN.

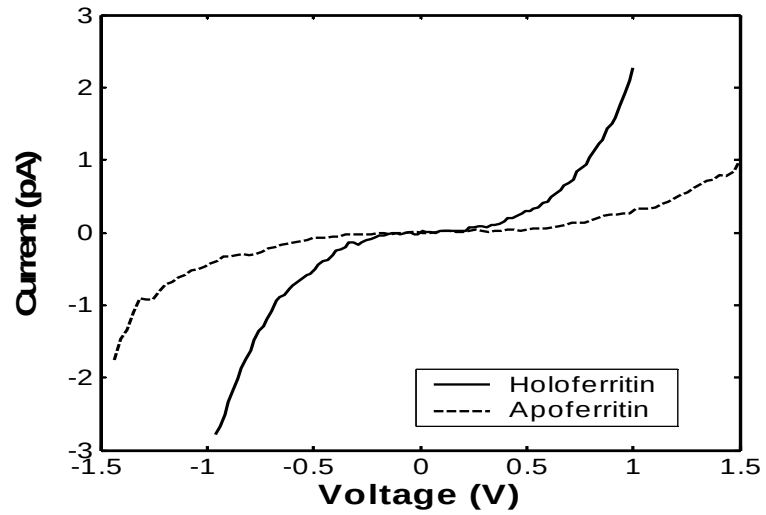

(a)

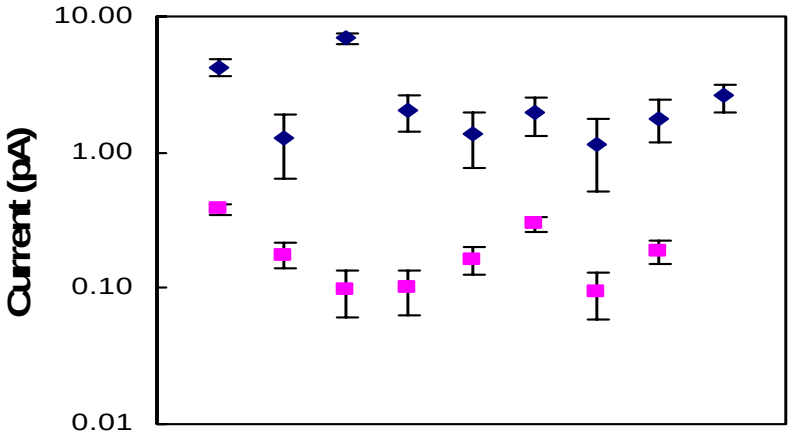

(b)

Figure 3-2. (a) The AFM I-V measurements of single holoferritin and apoferritin. The contact force between the AFM tip and the chosen ferritin was ~6 nN. To verify repeatability, the measurements were repeated 6 times with no appreciable change in the I-V curves. (b) The current through single holoferritins (♦) and apoferritins (■) at 1V

3.2 The Results of Gold Ball HoSF Measurements

There are several reasons why the variation in repeated measurements on the same molecule and in measurements on different molecules may be expected(see Figure 3-2 (b)) . Specifically, contact areas, contact forces, tip shapes, tip drift, and the orientation of the ferritin molecules relative to the tip will be different for different measurements. Simultaneous measurements on multiple molecules (films) provide more stable and lower noise I-V measurements for comparison with single molecule measurements. However the fabrication of a top electrode on ferritin layers by evaporation presents a major problem; holes are always present in the ferritin film that would lead to shorting between the top and bottom electrodes. As mentioned in Chapter 2, we overcame this problem by employing a 500μm diameter gold ball on a 100μm gold wire to make the top contact. The ball contact avoids the shorting problem and, in addition, does not subject the molecule to the high temperature of the metal evaporation process.

For gold ball ferritin I-V measurements, we use samples with a high coverage of ferritin molecules. We found that if we increase the ferritin density in the solution or the deposition time, there are more ferritin clusters or contamination particles formed on the sample surfaces. We needed to balance the ferritin concentration in the solution and the deposition time. The AFM images of the samples used for the gold ball measurements are shown in Figure 3-3.

The gold ball suspended from a gold wire was brought into contact with the sample surface and the contact force was increased until stable I-V curves could be measured. This required a force of 30~45 μN. An estimation of the force per ferritin molecule was made in order to allow comparison with the single molecule measurements. To do this, an estimate of the contact area between the film and the 500μm gold ball was required. Assuming a maximum deformation of the ferritin shell of 2nm, the contact area between the ferritin film and the gold ball surface would be ~3.1 μm^2. Since there are ~ 3.4×10^3 ferritin molecules in this area, the average force per molecule would be 8.8~13 nN. This range of forces agrees well with the 6~10 nN required for stable AFM measurements.

Figure 3-4 shows typical measurements for holoferritin and apoferritin films on gold measured with the gold ball contact. These curves were much more symmetric than the single ferritin curves measured with the AFM. Measurements with the gold electrode were taken at 16 different places on a holoferritin sample, yielding an average current of 0.60 ± 0.07 nA with 2 V applied. The average of 12 measurements on an apoferritin film yielded a current 0.11 ± 0.02 nA at 2 V. When the applied voltage was higher than 3 volts or the applied contact force was much higher than 45 uN, we had repeatability problems like those described above for the larger force and larger voltage AFM measurements.

The average current was 0.1nA with 1 V applied for the apoferritin. By considering the average current through a single ferritin (2.6pA) at 1 V from AFM measurements, it seemed there were only about 40 ferritin molecules contributing to the current under the gold ball. Based on this observation and the fact that the I-V

curves are approximately linear at low applied voltage (<0.3V), the estimated resistance of a single holoferritin molecule from the gold ball I-V measurements of holoferritin is ~ $8\times10^{12}\,\Omega$ at V~0 volt.

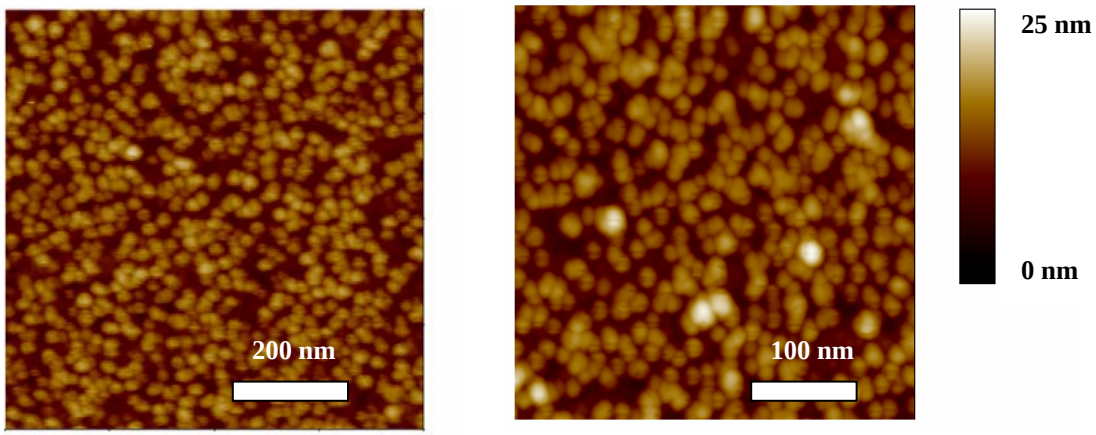

Figure 3-3. Tapping mode AFM image of apoferritin molecules (a) and holoferritin molecules (b) deposited on a flat gold surface with high ferritin density. The two samples were prepared by applying apoferritin and holoferritin solutions with concentration 1 mg/ml on flat gold surfaces for 20 minutes. These two samples were used for gold ball ferritin molecule conductivity measurements.

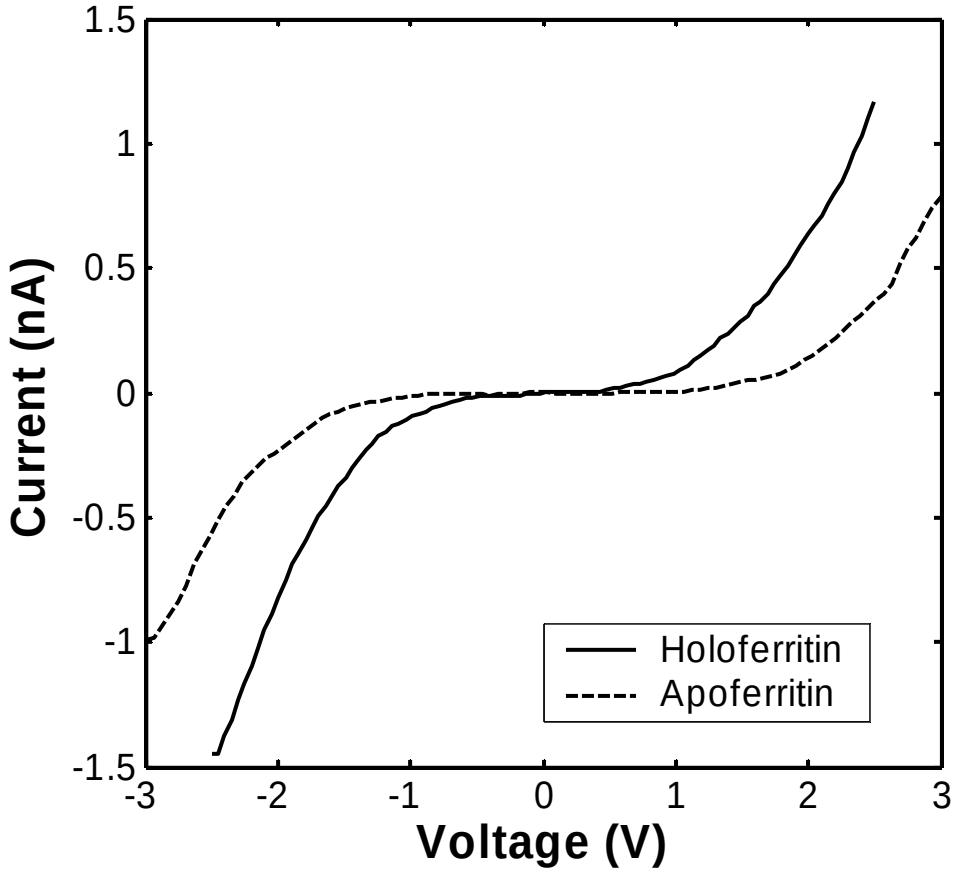

Figure 3-4. Current vs. voltage curves for holoferritin and apoferritin by using a gold ball with a diameter 500 μm. The ferritin density of the samples was ~1100/ μm^2. The contact force was ~45μN.

Chapter 4

I-V Measurements of Azotobacter Vinelandii Bacterial Ferritin

4.1 The Results of Single AvBF Measurements

Holo AvBF molecules deposited on the gold surface were imaged by tapping mode AFM for single ferritin I-V measurements as shown in Figure 4-1. The average height of the ferritin molecules in this image was 9.85±0.33nm based on the height measurement from 20 individual ferritin molecules. Single molecule I-V measurements were made on molecules whose height was close to the average molecular height for the sample of interest.

Typical I-V measurements on single ferritin molecules are shown in Figure 4-2 (a). The measured current and the applied voltage on the conductive tip showed a linear relationship. For most cases, the magnitude of the current measured for the single holo AvBF molecules was significantly larger than that measured for holo HoSP molecule at the same applied voltage. The shapes of measured I-V curves for holo AvBF and holo HoSF were also quite different. Figure 4-2 (b) shows the distribution of measured conductivity for holo AvBF. For each I-V measurement, the measured I-V curve was fitted to a straight line in the voltage range from -0.5 V to 0.5V and the conductivity is the slope of the fitted line.

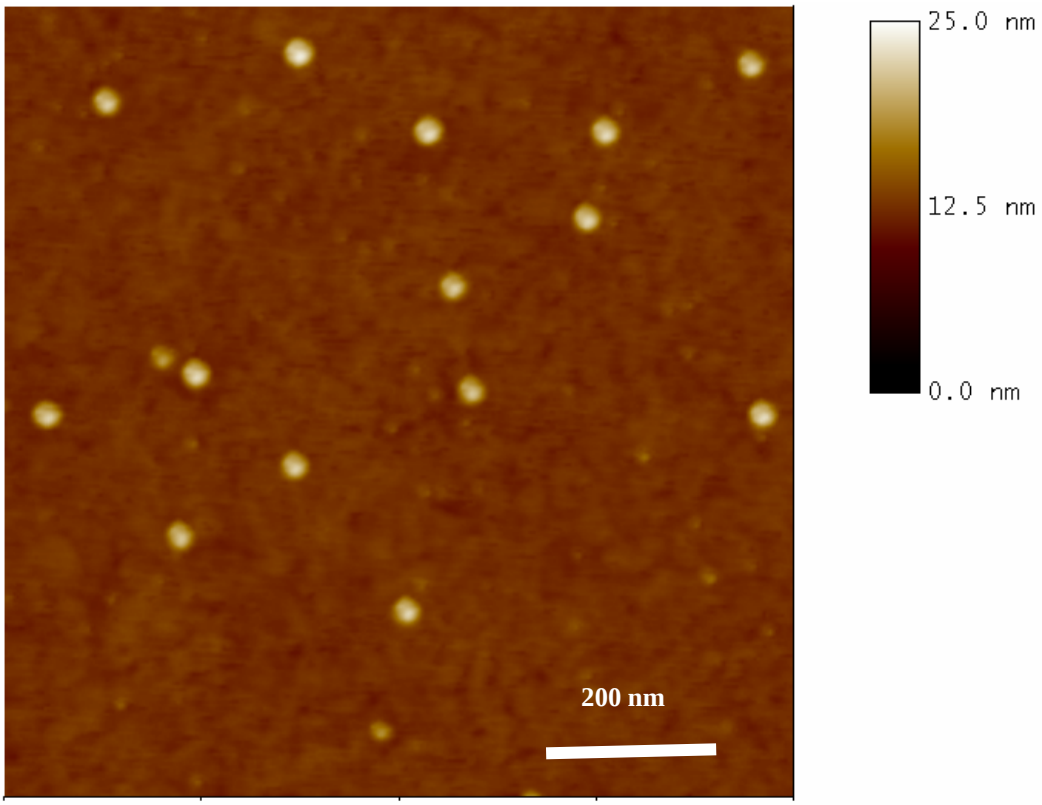

Figure 4-1. Tapping mode AFM image of holo AvBF molecules deposited on a flat gold surface with low ferritin density. This sample was prepared by applying holo AvBF solution with concentration 0.1mg/ml on flat gold surfaces for 10 seconds. This sample was used for single ferritin molecule AFM conductivity measurements.

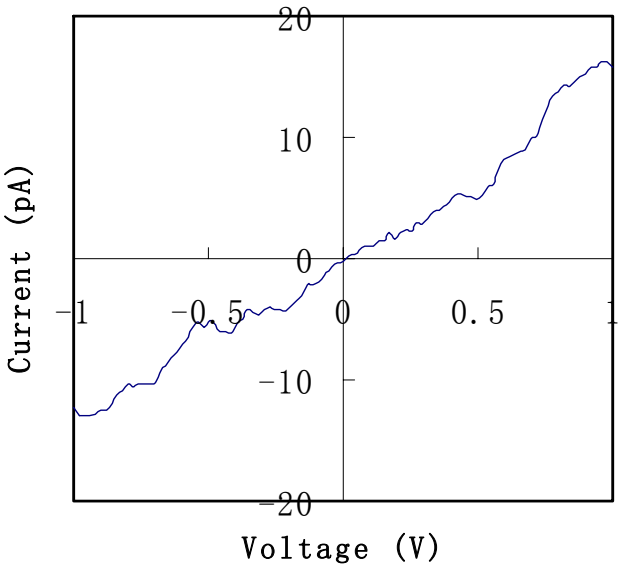

(a)

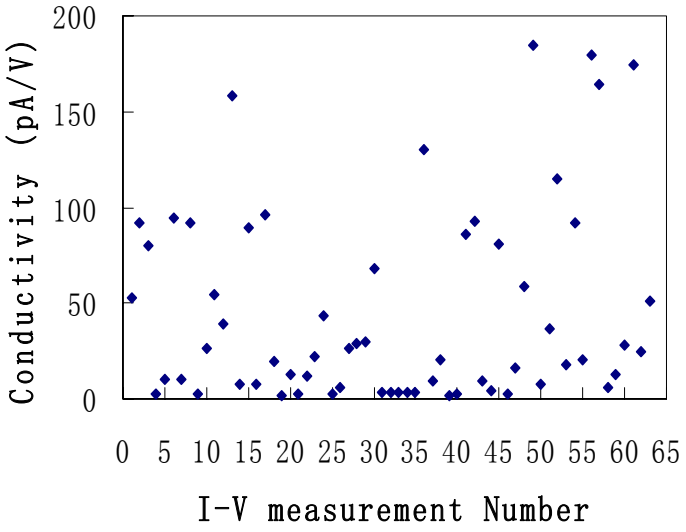

(b)

Figure 4-2. A typical I-V measurement of holo AvBF and the conductivity distribution. (a) A typical AFM I-V measurement of single holo AvBF. The contact force between the AFM tip and the chosen ferritin was ~6 nN. (b) The distribution of the measured conductivities of single holo AvBFs. The data presented here were all taken at applied forces in the range 6~10 nN. The results from 65 individual measurements are shown. The average conductivity was 45 pA/V.

The measured conductivity for single holo AvBFs showed large molecule to molecule variations. It varied from 2 to 185 pA/V. The average conductivity was 45 pA/V. We attribute this variation to different orientations of the ferritin molecules relative to the AFM tip and Au substrate. Generated heat was a significant issue, requiring voltage < 1V to obtain stable measurements.

4.2 The Results of Gold Ball AvBF Measurements

Based on the same consideration as for HoSF, we also performed I-V measurements on a thin film of holo AvBF deposited on a flat gold surface. Figure 4-3 shows the AFM image of the sample used for these measurements.

The contact force was kept in the range 30~45 μN when performing the I-V measurements. Figure 4-4 shows typical measurements for holo AvBF films on a flat gold surface measured with the gold ball contact. Measurements with the gold electrode in the range -2 V to 2V were taken at 10 different positions on the sample, yielding an average current of 28.0 ± 4.2 nA with 2 V applied. The same measurements in range –0.5 V to 0.5V were taken at 10 different positions on the sample, yielding an average current of 0.21 ± 0.03 nA with 0.5 V applied.

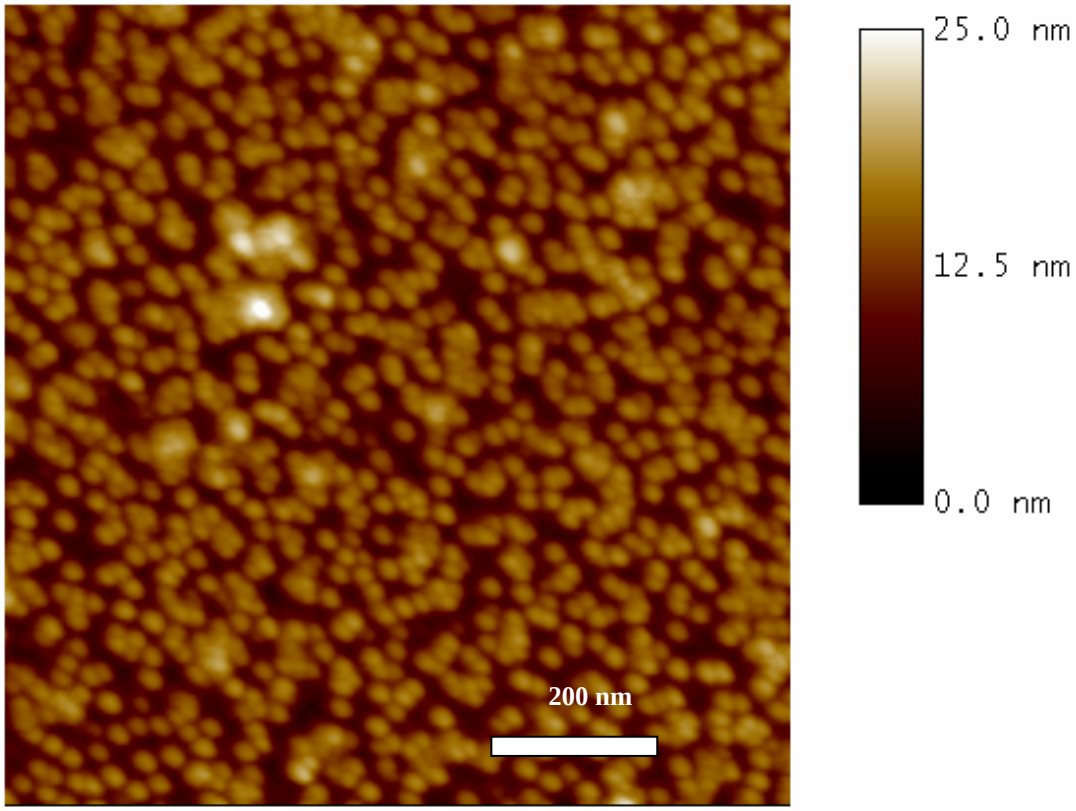

Figure 4-3. Tapping mode AFM image of holo AvBF molecules on flat gold surface with high ferritin density. The sample was prepared by applying a ferritin solution with concentration 1 mg/ml on flat gold surfaces for 20 minutes. The ferritin density was ~1200/μm^2. This sample was used for ferritin conductivity measurements by a 500μm gold ball as a contact probe.

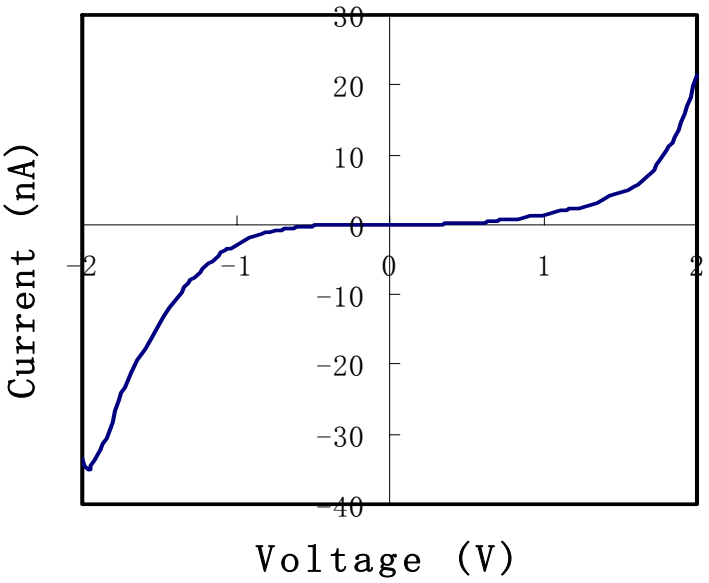

(a)

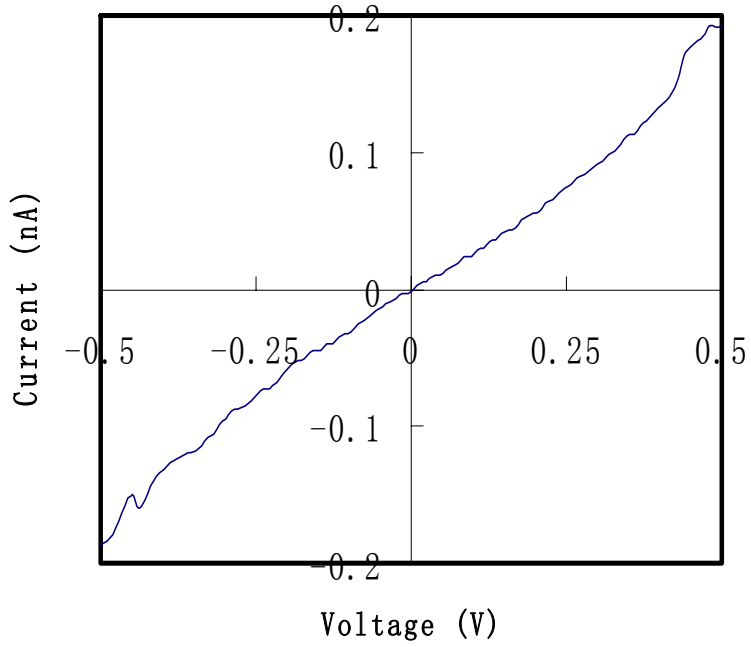

(b)

Figure 4-4. Current vs. voltage curves for holo AvBF using a gold ball with a diameter 500 μm. The ferritin density of the samples was ~1200/ μm^2. The contact force was ~45μN. (a) A typical I-V curve measured in the applied voltage range from -2V to 2V. (b) A typical I-V curve measured in the applied voltage range from -0.5V to 0.5V.

Chapter 5

Analysis of I-V Measurements of Ferritin

5 .1 Electrical Field Distribution between the AFM Tip and Au Substrate and the Attractive Force between Them

The electric field between the AFM tip and the Au substrate is not uniform. This non-uniformity will cause asymmetry in the ferritin I-V curves. The electric field also induces an attractive force between the tip and the sample, which may affect the I-V measurements. In this section, I will calculate the electric field and the attractive force between the AFM tip and the Au substrate in the vacuum environment without the presence of ferritin molecules. If the ferritin molecules are involved, the calculation will be more complicated. A simple vacuum calculation is used here to give an estimation of the magnitude of these effects[56]. The detailed calculation method is shown in Appendix 5.

Now suppose the top part of the conductive AFM tip has a radius 10nm, the separation between the tip and the flat Au surface is 10nm, and the tip and the Au surface are supplied one volt and zero volts respectively, then the attractive force between the tip and surface is: $F= 1.1\times10^{-11}$N. This force is much smaller than the applied force between the AFM tip and the samples. So we can neglect this force. The electric field and voltage distribution were calculated with a C program (Appendix 6). The results are shown in Figure 5-1. The effect of the uneven field distribution will be used in section 5.3.

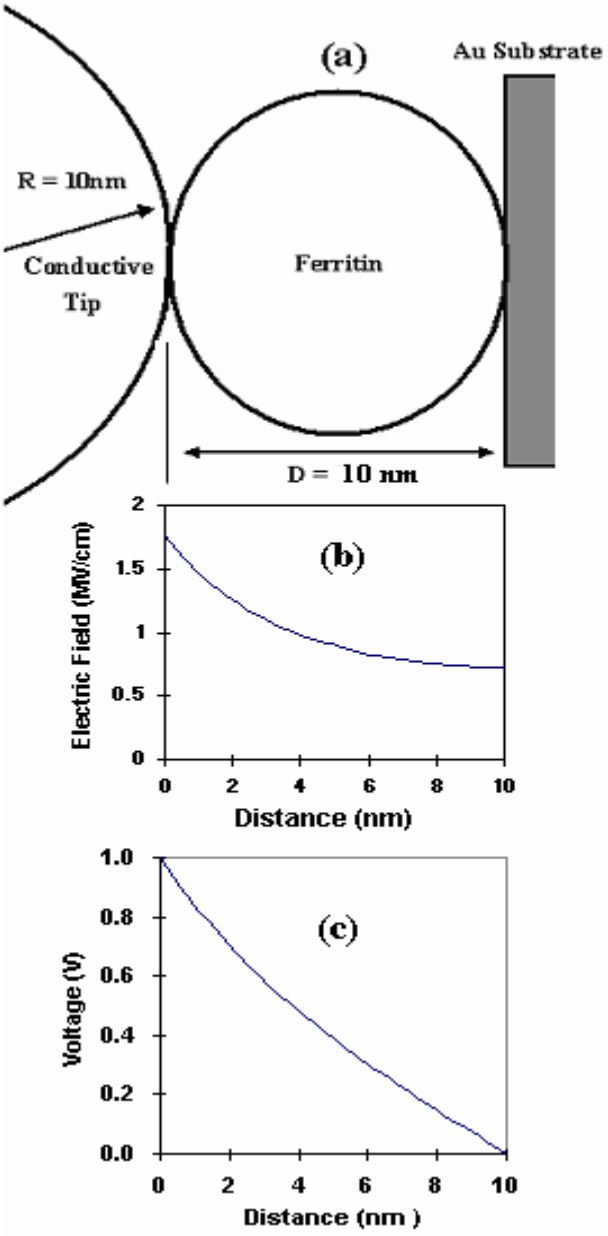

Figure 5-1. The distributions of the electric field and voltage between the conductive AFM tip and the flat Au substrate. (a) The relative positions of the tip(left), ferritin(middle) and Au substrate(right). The radius of the tip is 10nm and separation between the tip and the substrate is 10nm. (b) The electric field distribution in vacuum between the tip and substrate along the horizontal line passing through the center of ferritin. The electric field at the end of the tip is 1.77MV/cm. The surface electric field of the substrate right below the tip is 0.72MV/cm. The average electric field between the tip and the substrate is 1MV/cm. (c) The corresponding voltage distribution.

5.2 Common Models for Electron Transport Through Metal/Semiconductor and Metal/Insulator Interfaces

The shape of the measured I-V curves from HoSF strongly suggests a barrier for electron transport at the gold-ferritin interface. The barrier height at the interface of different material is an important parameter for electron transfer across the interface. We are especially interested in using models to describe the measured I-V curves and to determine the barrier height between the ferritin protein shell and the flat Au surface. There are two basic mechanisms for electron transport across a potential barrier: thermionic emission (Schottky emission) and electron tunneling. Thermionic emission happens when electrons have enough energy to pass over the potential barrier. When electrons don't have so high energy, tunneling is the main mechanism for electron transport across the potential barrier. We give a brief review of models for these two mechanisms and explore how they can be used to fit our measured I-V curves for getting the barrier height between the gold and the ferritin protein shell.

5.2.1 Schottky Emission

Schottky emission is usually used to explain the conductivity through a metal-semiconductor interface[57]. The potential barrier, which forms when a metal makes contact with a semiconductor, arises from the separation of charges at the metal-semiconductor interface such that a region depleted of mobile carriers is created in the semiconductor (shown in Figure 5-2). In the most simple case, the barrier height is given by the difference of work functions of the metal and semiconductor. In real junctions interface dipole layers and surface states also affect barrier height. The

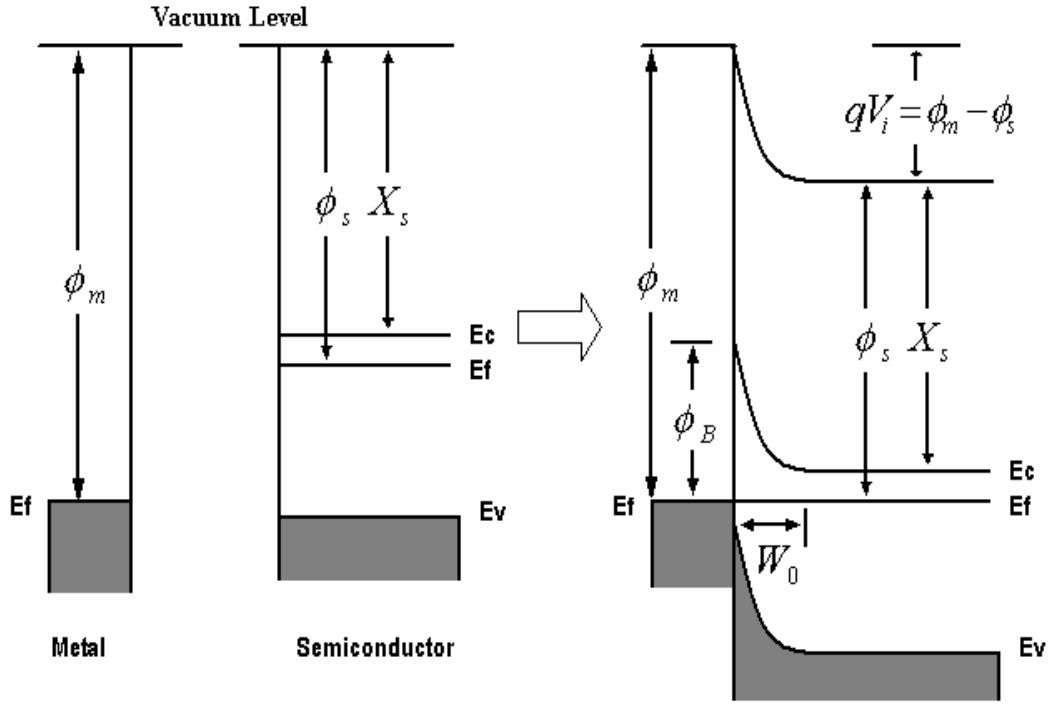

Figure 5-2. Electron energy band diagrams of metal contact to n-type semiconductor. The Schottky barrier height $\phi_B=\phi_m-\phi_s+Ec-Ef$. ϕ_m and ϕ_s are the work functions of the metal and the semiconductor respectively. Ef is the Fermi energy. Vi is the applied voltage. X_s is the electron affinity. Ec is the lowest electron energy in the conduction band and Ev is the highest electron energy in the valance band. W_0 is the width of the depletion layer.

current through the interface is controlled by two processes: first, thermionic emission over the barrier and second, drift and diffusion in the depletion region. The following current expression (Schottky diode equation) results from this model:

$$I(V) = I_0[\exp(-qV / nkT) - 1]$$

where

$$I_0 = SRT^2 \exp(-\frac{\Phi_B}{kT})$$

and

$$R = 4\pi m^* qk^2 / h^3 = 160 \frac{m^*}{m} Acm^{-2}K^{-2}$$

S is the contact area and n is called the "ideality factor" giving by:

$$\frac{1}{n} = 1 - \partial\Phi_B / \partial V = \frac{kT}{q}\frac{d}{dV}\ln[J /(1 - \exp(-qV / kT))]$$

For V>3kT/q,

$$\frac{1}{n} = \frac{kT}{q}\frac{d(\ln J)}{dV}$$

The barrier height can be obtained by fitting the measured V-I curves to the equation

$$I(V) = C[\exp(-DV) - 1]$$

to determine C and D, and barrier height is given from C as follows:

$$\Phi_B = kT \ln(A_{eff} RT^2 / C)$$

Occasionally, Schottky emission is also used to explain the current through metal-insulator interfaces[58]. For our metal-ferritin-metal case, if we apply the

Schottky emission model to our measurements, there will be two Schottky junctions in series. One is forward biased and the other one is reverse biased. Assume one is forward biased with voltage V_1, the other is reverse biased with V_2. Also assume the contact area between the ferritin and the AFM tip and the contact area between the ferritin and the flat Au surface are the same, then:

$$I = C(\exp(\frac{qV_1}{nkT}) - 1) = C(1 - \exp(-\frac{qV_2}{nkT}))$$

Since $V_1+V_2=V$, we can obtain the equation:

$$I = C\frac{\exp(\frac{qV}{nkT}) - 1}{\exp(\frac{qV}{nkT}) + 1}$$

The functional form of this equation as shown in Figure 5-3 is significantly different than the form of our measured I-V curves. Schottky emission is not a good description of the mechanism for current transport over the metal-ferritin-metal interface barrier.

5.2.2 Tunneling Models

There are two basic models for electron tunneling: Fowler Nordheim (FN) tunneling and Simmons tunneling. The FN current equation form FN tunneling model is applicable for the case when the applied voltage is larger than ϕ_B/e. For simplicity, we only consider the Simmons current equation (from Simmons tunneling model) for a rectangular potential barrier even though Simmons tunneling is applicable for any potential barrier. For the case when the applied voltage is larger than ϕ_B/e, the

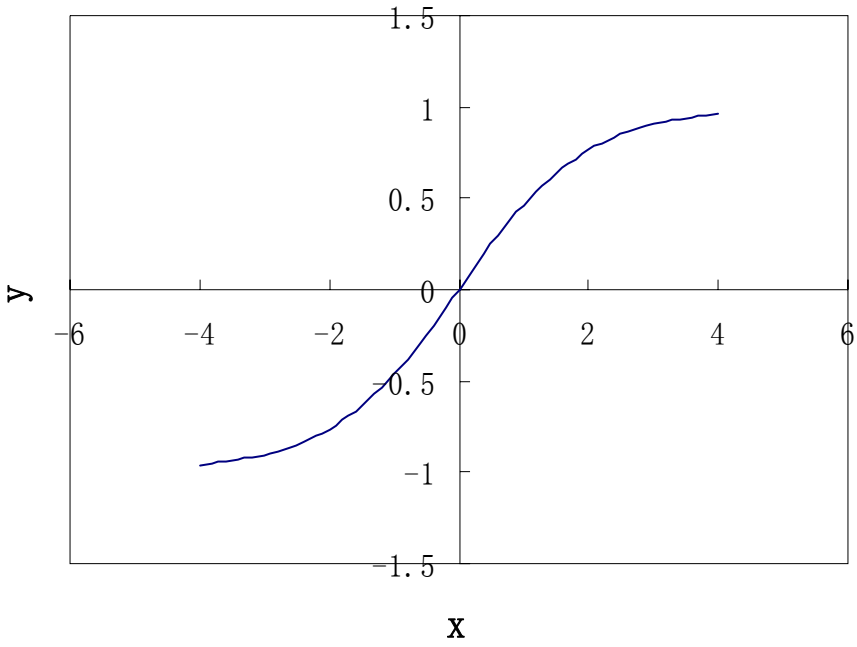

Figure 5-3. The functional form of y = [exp(x)-1]/[exp(x)+1].

Simmons current equation is essentially the same as the FN current equation. What we used here was the Simmons current equation for the case when the applied voltage is less than ϕ_B/e since the FN current equation is not applicable in this voltage range. There are no analytical current equations for the case when the applied voltage is around ϕ_B/e. Since we didn't know the barrier height, we used both Simmons current equation and FN current equation to fit our measured I-V curves and to see which one gives a better fit.

Fowler Nordheim Tunneling

Fowler-Nordheim (FN) tunneling (tunneling emission or field emission) theory is a widely used model to describe electron tunneling from a metal's Fermi energy over a barrier into an adjacent insulator[59]. FN tunneling was originally used to explain the phenomenon of the extraction of electrons from cold metals in intense electric field in air or in vacuum environments. Later it was modified to explain electron tunneling across the metal-insulator interface. The explanation here most closely follows that of reference 59.

FN theory is one-dimensional. It assumes the interface has a step potential energy barrier :

$V(x)=0$, when $x<0$;

$V(x)=C$, when $x\geq 0$, where C is a positive constant.

The current caused by the tunneling electrons is found by integrating(over all the electron energies) the product of the equilibrium flux of electrons (in metal) incident on the interface and the probability of electron tunneling through the barrier:

$$I = -qS\int_0^{\infty} N(K)D(K)dK$$

where S is the contact area, q is the electron charge, N(K) is the flux of electrons with kinetic energy K in the x direction and D(K) is the probability of electron tunneling. Since the flux of electrons in the x-direction and with x-momentum in the interval between p_x and $p_x + dp_x$ is:

$$N(p_x)dp_x = \int_{-\infty}^{+\infty}\int_{-\infty}^{+\infty} \frac{2p_x}{mh^3} \frac{dp_y dp_z}{\exp(\frac{\varepsilon - E_f}{kT}) + 1} dp_x$$

$$= \frac{2}{h^3} dK \int_{-\infty}^{+\infty}\int_{-\infty}^{+\infty} \frac{dp_y dp_z}{\exp(\frac{K - E_f}{kT} + \frac{p_y^{\,2} + p_x^{\,2}}{kT}) + 1}$$

$$= N(K)dK$$

E_f is the Fermi energy of electron in the metal. The following equation can be derived:

$$N(K) = \frac{4\pi mkT}{h^3} \ln(1 + \exp(\frac{K - E_f}{kT}))$$

From the WKB approximation,

$$D(K) = \exp(-2\int_{x_1}^{x_2} \frac{\sqrt{2m^*(V(x) - K)}}{\hbar} dx)$$

where x_1 and x_2 ($x_2 > x_1$) are the two solutions of the equation: V(x)=K.

Here we will neglect the effects of finite temperature and image charge. The effect of image charge in some situation can cause a big difference; however, in our case it is not significant (as shown in Appendix 7). The following equation is obtained for the tunneling current[60-63]:

$$I(E) = \frac{A_{eff} q^3 E^2 m^*}{8\pi h \Phi_B m} \exp\left[\frac{-8\pi\sqrt{2m^*}\Phi_B^{3/2}}{3hqE}\right]$$

where A_{eff} is the effective contact area, E is the applied electric field, Φ_B is the contact barrier height (Φ_B = C-E_f), and q, m^*, m, and h are electron charge, effective mass of the electron, free electron mass, and Plank constant respectively. If we assume E=V/d, where V is the applied voltage, and d is the separation between the two electrodes, then:

$$I(V) = A * V^2 \exp(-B/V)$$

where A and B are given as follows:

$$A = \frac{A_{eff} q^3 m^*}{8\pi h \Phi_B d^2 m}$$

$$B = \frac{8\pi\sqrt{2m^*}\Phi_B^{3/2} d}{3hq} = 6.83 d \left(\frac{m^*}{m}\right)^{1/2} \Phi_B^{3/2} (Volts)$$

Here the units of d and Φ_B are nm and eV respectively. Since we don't know the effective contact area, the constant A is not very useful for us. We are interested in the constant B, from which we can get an expression for the barrier height Φ_B.

There is a simple way to get the exponential factor in the above FN equation from the WKB approximation. This simple method can give us some physics insight to see how this exponential factor is generated. Suppose an electron with kinetic energy K meets a triangular potential barrier with a barrier height ϕ_B (shown in

Figure 5-4) and the electron needs to tunnel through a distance L to pass through the potential barrier. From the WKB approximation, we can get the electron tunneling probability:

$$D = \exp(-2\int_0^L \frac{\sqrt{2m^*[V(x)-K]}}{\hbar}dx)$$

where m* is the effective mass of electron. Since V(x)-K= ϕ_B(1-x/L), we can get

$$D = \exp(-\frac{8\pi\sqrt{2m^*}\Phi_B^{3/2}}{3qhE})$$

where E=ϕ_B/L.

Simmons Tunneling

In FN tunneling, electron transport back over the barrier is ignored. For metal-insulator-metal junctions, a more general tunneling current is given by[64]:

$$J = 4\pi\frac{em}{h^3}\int_0^\infty dE(f_c(E)-f_a(E))\int_0^E P(E_x)dE_x$$

where

$$f_c(E) = (1+\exp(\frac{E-E_f}{kT}))^{-1}$$

and

$$f_a(E) = (1+\exp(\frac{E+eV-E_f}{kT}))^{-1}$$

are the electron distribution in the cathode and anode electrodes respectively; E_f is the Fermi energy of the cathode; V is the applied voltage between the cathode and anode; E and E_x are the energy and 'x-directed' energy of the electron respectively; and P(E_x)

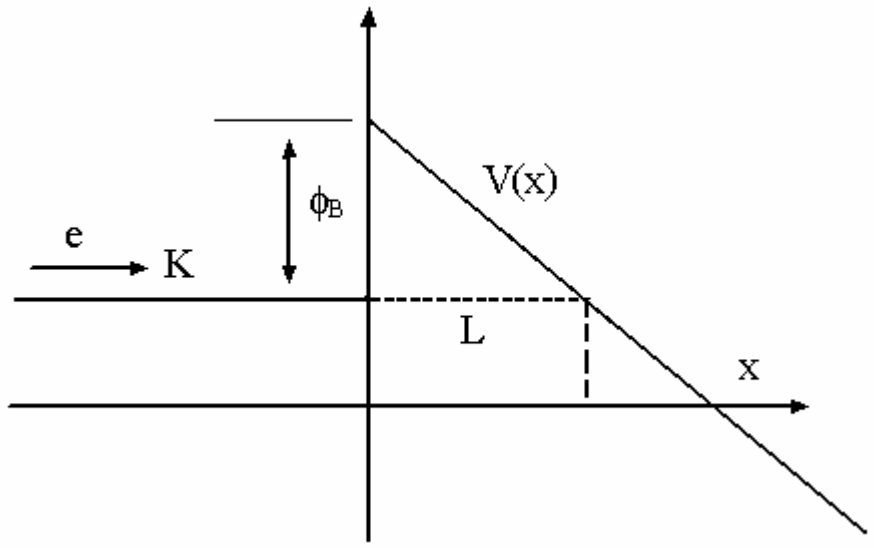

Figure 5-4. An electron with energy K tunneling through a triangular potential barrier with a barrier height ϕ_B.

is the electron tunneling probability through the insulator. By using the above equation, Simmons obtained a general current formula for electron tunneling through any arbitrary potential barrier[65] for metal-insulator-mental junctions as shown in Appendix 8.

For a rectangular potential barrier witha barrier height ϕ_B, Simmons tunneling can give the following current equation when $V<\phi_B/e$:

$$I = A\{(\phi_B - \frac{eV}{2})\exp[-B(\phi_B - \frac{eV}{2})] - (\phi_B + \frac{eV}{2})\exp[-B(\phi_B + \frac{eV}{2})]$$

where

$$A = \frac{A_{eff} e}{2\pi h s^2}$$

$$B = \frac{4\pi s(2m)^{1/2}}{h}$$

A_{eff} is the effect contact area and s is the separation of the two metal electrodes.

5.3 Analysis for I-V Measurements of Horse Spleen Ferritin

We used the Simmons tunneling equation and the FN tunneling equation to fit the measured I-V curves from HoSF as shown in Figure 5-5. We explored a wide range of parameters and the best fits are shown in this figure. As seen in the figure, the FN tunneling equation gives a much better fit than the Simmons tunneling equation. In this section, we used FN tunneling equation to fit all our measured I-V curves from HoSF.

The fitted B values for the single ferritin I-V measurements are shown in

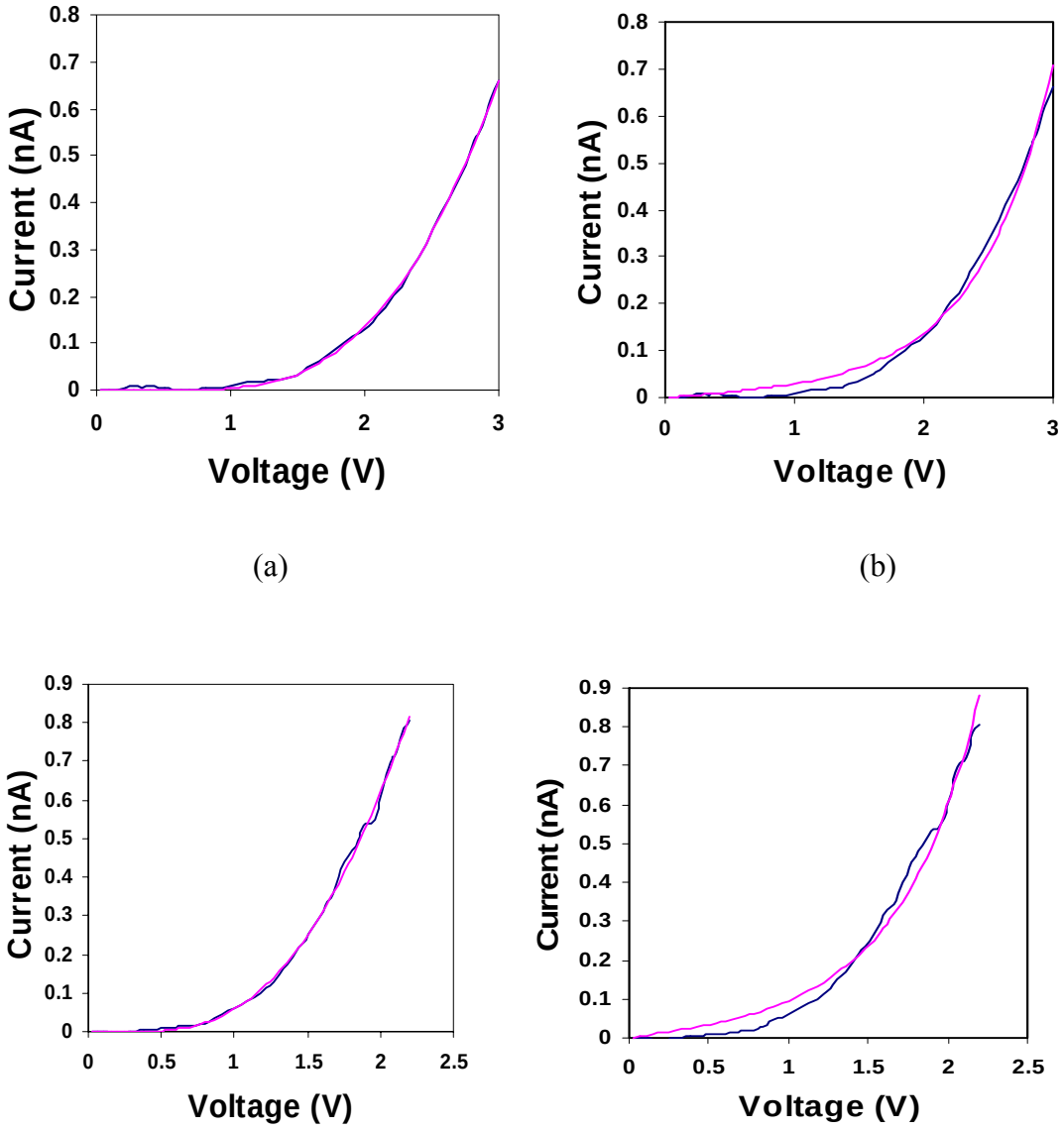

Figure 5-5. Comparison of the fits of the measured I-V curves from horse spleen ferritin to the FN equation and the Simmons equation. (a) The fit of an I-V curve from gold ball measurement on horse spleen apoferritin to the FN equation. (b) The fit of the same I-V curve in (a) to the Simmons equation in the intermediate voltage range. (c) The fit of an I-V curve from gold ball measurement on horse spleen holoferritin to the FN equation. (d) The fit of the same I-V curve in (c) to the Simmons equation in the intermediate voltage range.

Figure 5-6. The average B value of apoferritin is about 2.4 times higher than average B value of holoferritin. For the gold ball I-V measurements of ferritin films, by fitting the measured I-V curves to FN theory, the B values were 2.07 ± 0.32 V for holoferritins and 5.16 ± 1.02 V for apoferritins. The average value of B for apoferritins is about 2.5 times larger than the average B value of holoferritins.

The ratios of the B values for holoferritin vs apoferritin from the single molecule AFM-based and gold ball measurements are close; however, the average B values measured by the AFM were about 2.2 times larger than the average B values measured by the Au ball. A larger B value is expected from the sharp AFM tip measurements due to the non-uniformity of the electric field (shown in Figure 5-7 (a) and (b)). The non-uniform field yields a wider potential barrier for the tunneling electrons and a larger corresponding B factor. A quantitative analysis of the non-uniformity would require a detailed computational study.

All the measured I-V curves showed some asymmetry. This can also explained by the non-uniformity of the electric field between the tip and the Au substrate (Figure 5-7 (a), (b) and (c)). If a positive voltage is applied to the tip, electrons contributing to the tunneling current have to tunnel through a wider potential barrier than the case of a negative tip voltage. Since the electric field is more uniform for the gold ball measurements, the measured I-V curves were more symmetric than those from AFM measurements.

Using the average fitted B value for apoferritin of 5.2 volts and the ferritin height of ~ 10 nm (as measured by tapping mode AFM), FN theory yields a barrier height:

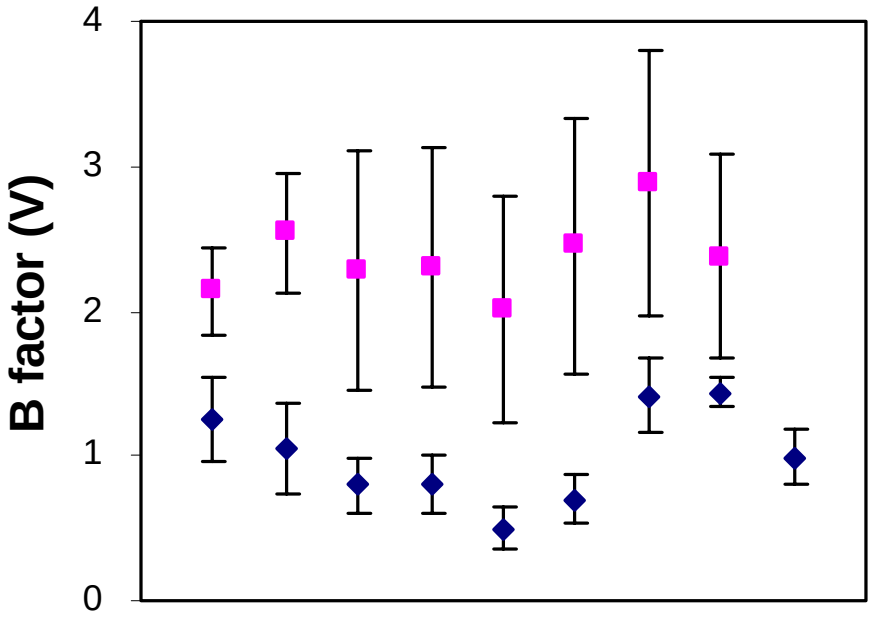

Figure 5-6. The fitted Fowler Nordheim B factors for the I-V curves of nine holoferritin (♦) and eight apoferritin (■) molecules.

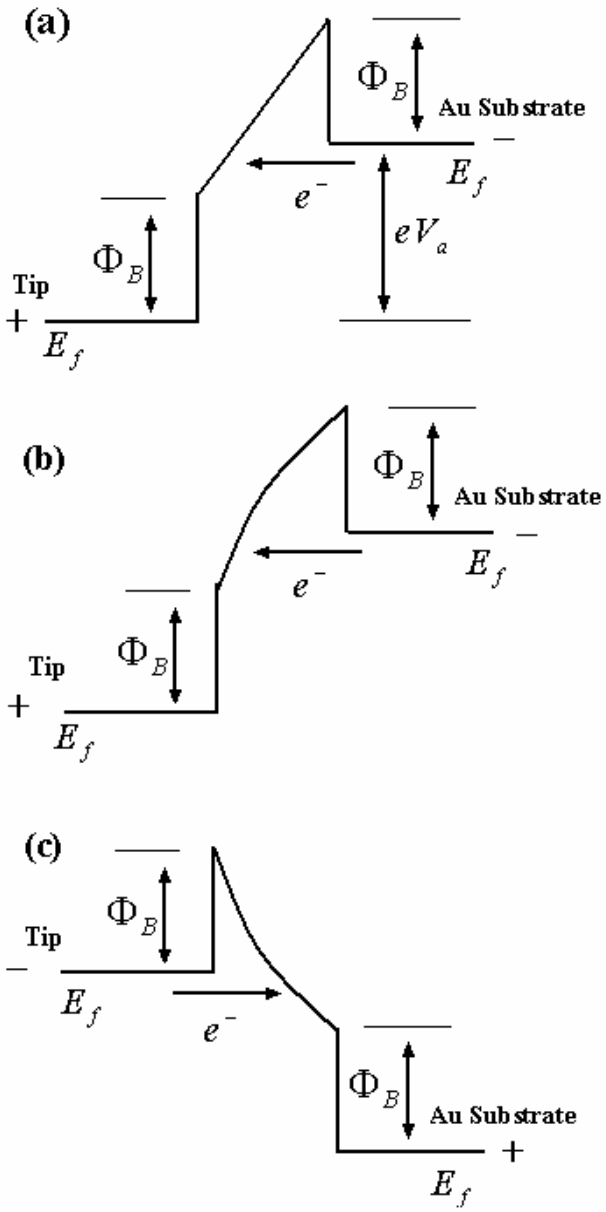

Figure 5-7. Energy level diagram for the Au-coated tip, ferritin and the flat Au substrate. (a) The energy bands between the tip and substrate assuming the electric field between the tip and substrate is even. E_f is the electron Fermi energy inside the Au and Φ_B is the barrier height between Au and ferritin. eV_a is the applied potential energy difference between the AFM tip and Au substrate. Electrons at the Fermi energy tunnel the triangular potential barrier. (b) If the non-uniformity of the electric field is considered, electrons tunnel through a wider potential barrier than the triangular potential barrier when the tip is positive relative to the substrate. (c) Electrons see a narrower potential barrier than the triangular potential barrier when the tip is negative relative to the substrate.

$$\Phi_B = 0.19(\frac{m}{m^*})^{1/3} eV$$

The effective mass of the protein shell is not known; however, the barrier height depends on this value somewhat weakly.

As holoferritin is much more conductive than apoferritin, the core of holoferritin must present a smaller barrier to electron transport than the ferritin protein shell. For holoferritin we use a double barrier model as shown in Figure 5-8 (a). The lower LUMO energy of the core relative to the shell is due to the higher conductivity observed in holoferritin. The voltage drop across the ferritin core is much smaller than the voltage drop across the protein shell. The potential barrier associated with the protein shell (see Figure 5-8 (b)) is the dominant barrier to electron conduction. If we neglect the potential drop across the more conductive core, the electric field inside the protein shell is $E \approx 2V/d_1$, where d_1 is the thickness of the protein shell (~2nm) (Figure 5-8 (a)). The B factor for holoferritin is then given by:

$$B = \frac{8\pi\sqrt{2m^*}\Phi_B^{3/2} * (2d_1)}{3hq} = 6.83 * (2d_1)(\frac{m^*}{m})^{1/2}\Phi_b^{3/2}$$

For apoferritin we use a single barrier model as shown in Figure 5-8(c). The B factor for apoferritin is:

$$B = 6.83D(\frac{m^*}{m})^{1/2}\Phi_b^{3/2}$$

where D is the effective barrier width. We use the AFM measured height of the apoferritin molecule (~10 nm) for the effective barrier width D. The calculated ratio of the B factor for apoferritin to the B factor for holoferritin is 2.5, in good agreement with the experimental results (2.4 by AFM and 2.5 by gold ball).

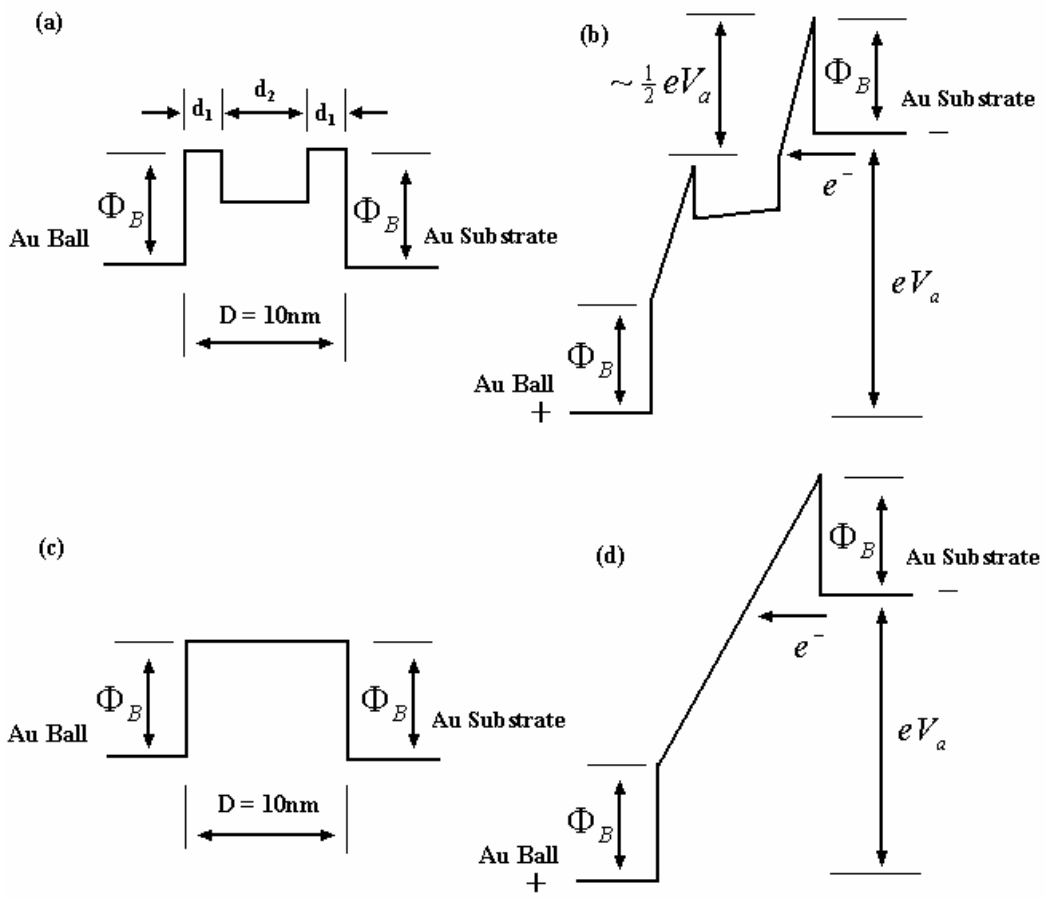

Figure 5-8. Electron energy levels for gold ball ferritin conductivity measurements. (a) The energy band structure for Au ball, holoferritin and Au substrate with no applied voltage. Φ_B is the barrier height between Au and ferritin protein shell. D is height of holoferritin under the contact of the gold ball. d_1 is the thickness of the protein shell and d_2 is the diameter of the ferritin core. (b) The energy band structure for Au ball, holoferritin and Au substrate with a positive applied voltage relative to the Au substrate. eV_a is the applied potential energy difference between the Au ball and Au substrate. Since the ferritin core is more conductive than the protein shell, most applied voltage is dropped on the protein shells and each protein layer right below the AFM tip holds one half of the applied voltage. (c) The energy band structure for Au ball, apoferritin and Au substrate with no applied voltage. (b) The energy band structure for Au ball, apoferritin and Au substrate with a positive applied voltage relative to the Au substrate.

5.4 Discussion of I-V Measurements of Bacterial Ferritin

Here we compare the conductivities of holo AvBF and holo HoSF. The average conductivity for a single holo AvBF was 45 pA/V. The average current for a single holo HoSF was 2.6pA at 1V. Holo AvVF is ~17 times more conductive than holo HoSF at 1V. The average current for the holo AvBF film and for holo HoSF film at 2V were 28.0nA and 0.60nA respectively from the gold ball I-V measurements. Holo AvBF is ~47 times more conductive than holo HoSF at 2 V.

Even though the protein subunits of holo HoSF and those for holo AvBF are not identical (Holo HoSF has both L subunits and H subunits while holo AvBF has only H subunits), we don't expect their electrical properties to be significantly different. The main difference that should affect conductivity is the 12 heme groups in the holo AvBF protein shell. Each heme group is located in the middle of two subunits, contacting the mineral core and extending toward the outer surface of the protein shell. The structure of the heme group (protoporphyrin IX) is shown in Figure 5-9. In the frame (the ring like portion) of a heme, each carbon atom has sp^2 hybrid orbitals and an unhybridized p_z orbital. The two unhybridized p_z orbitals from the nearby carbon atoms form a pi bond (from sideways overlap of two p_z orbitals). Since each unhybridized p_z orbital only holds one electron (half full), the nearby carbon atoms can exchange electron easily by the pi bond between them. The pi bonds (which essentially are delocalized electron wave functions) in the heme frame should make it be more conductive than the protein shell. We believe that electron transport through the heme group is the main cause of the conductivity difference between holo HoSF

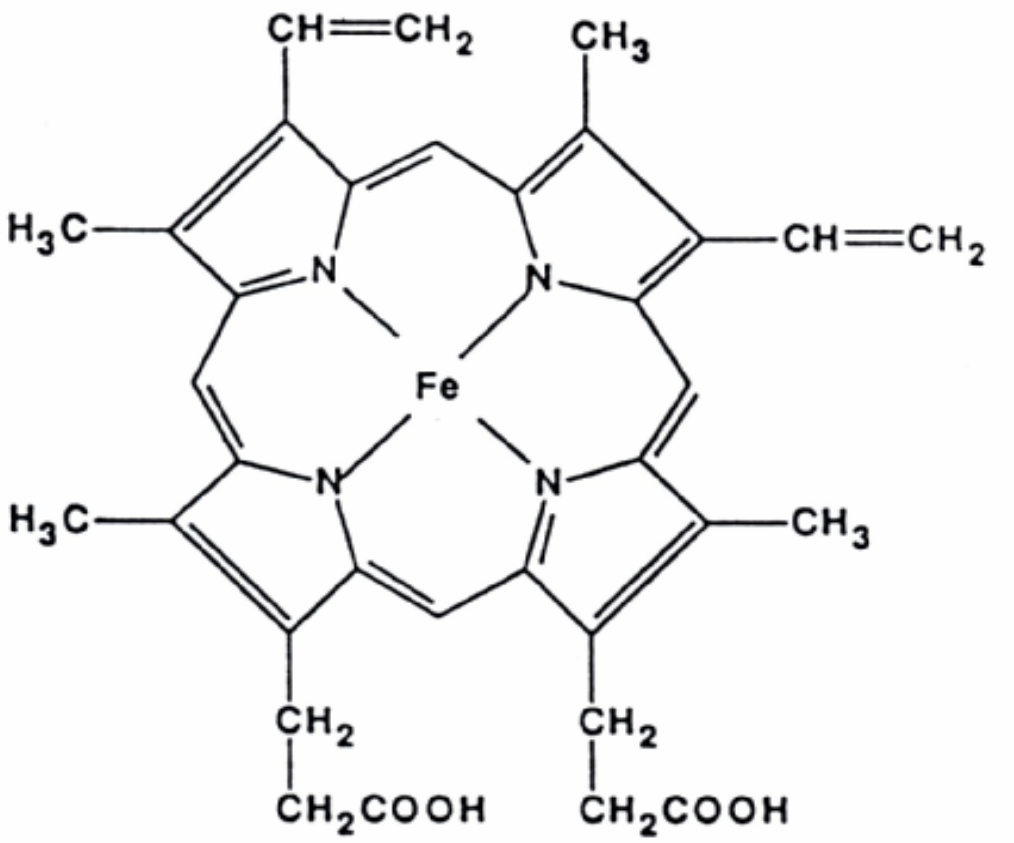

Figure 5-9. The structure of a heme group (formula: $C_{34}H_{32}N_4O_{10}Fe$) in AvBF protein shell.

and holo AvBF. Under the pressure of the AFM tip, heme groups may directly connect the ferritin core and two electrodes. Even if heme groups doesn't connect the core and the electrodes, the tunnel distance (to the heme) will be significantly shorter than the tunnel distance in the HoSF. Whether the electron sees a tunnel barrier or not, in the case of AvBF, the electron conduction should be higher than in the case for non-heme hoho HoSF, for which electrons have to tunnel through the protein shell.

At low voltage (V<0.3 volt), both the measured currents from the holo AvBF and from holo HoSF have a linear relationship with the applied voltage. The resistance for Holo AvBF and HoSF are ~$2\times10^{10}\,\Omega$ and $5\times10^{12}\,\Omega$ respectively.

For battery applications, ferritin conductivity at low voltage (<<1V) is a particular concerns. At low voltage, the conductivities of apo and holo HoSF show no big difference. The conductivity along the outer protein surface could be a significant contribution to the measured conductivity. Since the measured current for holo AvBF is much larger than that for holo HoSF and there is no essential difference in the surfaces of these two kinds of ferritin molecules, most of the measured current for holo AvBF must go through the ferritin protein shell.

The voltage drop across the ferritin protein shell has been a significant concern for battery applications. The current density for a typical battery is ~1mA/cm^2. If we assume that the density of ferritins on the flat gold surface is $1000/\mu\text{m}^2$ and each ferritin equally contributes to the current, the current through each ferritin molecule would be ~10^{-2} pA. Then the voltage across each holo AvBF is ~2×10^{-4}V. Such a small voltage drop across the holo AvBF won't affect the performance of batteries based on AvBF.

Chapter 6

Conclusions and Recommendations

6.1 Conclusions

We measured the electrical conductivity of single horse spleen ferritins (HoSFs) and azotobacter vinelandii baterial ferritins (AvBFs) successfully by conductive AFM(c-AFM). This was done using a novel combination of a tapping mode AFM and a script program, which positions the AFM tip on a single ferritin molecule for current-voltage measurements.

We also developed a new method to measure the conductivity of a thin film of ferritin molecules by using a gold ball to provide a micron scale contact between the gold ball and the ferritin film.

The conductivity measurements show that the protein shell of HoSFs acts as a significant tunneling barrier for electron transfer. The average currents measured for holo (with mineral core) HoSF molecules were 5 and 13 times larger than that measured for apo (with empty core) HoSF molecules as measured by gold ball at 2V and c-AFM at 1V respectively. This significantly higher conductivity in holoferritin indicates that the core is more conductive than the shell, and that conduction through the shell is likely the main factor limiting electron transfer.

The measured I-V curves for single ferritin molecules are sensitive to the applied contact force and the applied voltage range. In order to get stable

measurements, we had to carefully control these two parameters. For our measurements, we limited the contact force in the range of 6nN ~ 10nN and used applied voltages less than 1.5V for single ferritin measurements.

We used FN theory to fit our measured I-V curves from the HoSF. From the fitted constants, we obtained the following expression for the barrier height ϕ_B between gold and the ferritin protein shell:

$$\Phi_B = 0.19(\frac{m}{m^*})^{1/3} eV$$

where m* and m are the effective mass of electron in the ferritin protein shell and the free electron mass. We used a double barrier model for holo HoSF and a singe barrier model for apo HoSF to successfully explain the difference of the fitted constants from holo HoSF and apo HoSF respectively.

The measured I-V curve from ferritin molecules were asymmetric. This phenomenon was explained by the non-uniformity of the electric fields between the AFM tip and the Au substrate.

The average currents measured for holo AvBF were 47 and 17 times larger than that measured for holo HoSF molecules as measured by gold ball at 2V and c-AFM at 1V respectively. Heme groups in holo AvBF are the main cause of such a big difference. The pi bonds in the heme frame make it more conductive than the protein shell. These heme groups provide the main path for electron transport across the protein shell in AvBF.

For battery applications, the estimated voltage drop across each holo AvBF is ~2×10^{-4}V. Such a small voltage drop across the holo AvBF won't affect the

performance of batteries based on AvBF. This is a good news; in the case of bacterial ferritin, the protein shell conductivity is far higher than required when compared to today best battery materials. Now the main question is: can the core material perform as well as the shell?

6.2 Recommendations for Future Works

It may be possible to modulate electron transfer in mammalian ferritin by modifying the protein shell. Apo mammalian ferritin contains six redox centers in the protein shell[46]. These redox centers are proposed as conductive pathways through the protein shell. If we introduce more redox centers, the conductivity of the protein shell may increase significantly. The ferritin conductivity experiments would be a test of redox center conductive pathway model.

The barrier height between the electrode and the protein shell affect the conductivity greatly. We may change the barrier height through the use of a contact electrode material with a work function lower than that of gold.

Not too much is known about the conductivity of the ferritin core. If we replace the ferritin core with Au or Pt, it will be easier to study the conductivity of the ferritin protein shell by eliminating the unknown conductivity of the ferritin mineral core. This core replacement is being done with other metals[42] and may be soon be possible with noble metals.

We attempted to measured the conductivity of apo AvBF. However, the apo AvBFs would not assemble on the gold surface. Bacterial ferritin protein may have been damaged in the core extraction process. Future measurements on apo AvBF

measurements would be valuable for comparison with our measurements on holo AvBFs. There is also no previous work measuring the conductivity of the ferritin core. If the conductivity of the ferritin core were measured independently, it would help in the analysis of the conductivity of the protein shell.

These conductivity measurements of ferritin molecules were performed in the ambient environment. Similar conductivity measurements performed in a buffer liquid would be advantageous in determining the conductivity in a system closer to a physiological environment.

There are ~80,000 atoms in the ferritin protein shell. The complete computation of ferritin molecule conductivity is beyond contemporary first principle computational abilities (up to 4000 atoms). But for AvBF, the electronic energy levels and the conductivity of the heme group in contact with gold could be computed by the first principle methods. These computations could aid in a more in depth analysis of these conductivity measurements.

References

[1] Pauline M. Harrison, Paolo Arosio. Biochim. Biophy. Acta. **1996,**1275, 161-203.

[2] Theil, E. C. Ann. Rev. Biochem. **1987**, 56, 289-315.

[3] J. W. Drysdale. Ciba Found. Symp. **1977**, 51, 41-57.

[4] Robert F. Weaver. Molecular Biology (second edition). McGraw-Hill Higher Education. **2002**.

[5] J. L. White, J. M. A. Smith, P. M. Harrison. Inorg. Biochem. **1983**, 5, 39-50.

[6] S. H. Banyard, D. K. Stammer, P.M. Harrison. Nature. **1980**, 288, 298-300.

[7] M. Heusterspreute, R. R. Crichton. FEBS Lett. **1981**, 129, 322-327.

[8] G.C Ford, P. M Harrison, D. W. Rice, etc. Philos. Trans. R. Soc. London Ser. **1984**, B 304:561-565.

[9] S. Levi, P. Santambrogio, B. Coris, etc. Biochemical J. **1996**, 317(2), 467-473.

[10] A. Treffry, E. R. Bauminger, D. Hechel, etc. Biochem. J. **1993**, 296(3), 721-728.

[11] A. Treffy, P.M. Harrison, A. Luzzago, etc. FEBS Lett. **1989**, 247(2), 268-272.

[12] E. I. Stiefel and G. D. Watt. Nature. **1979**, 279, 81-83.

[13] T. D. Rechards, K. R. Pitts. G. D. Watt. J. Inorg. Biochem. 1**996**, 61(1), 1-13.

[14] G. D. Watt, J. W. McDonald, C. H. Cui, K. R. N. Reddy. J. Inorg Biochem. **1993**, 51(4), 745-758.

[15] J.M. Cowley, Dawn E. Janney, etc. J. Structural Bio. **2000**, 131, 210-216.

[16] F.A. Fischbach, P.M. Harrison, and T. G, Hoy. J. Mol. Biol. **1969**, 39, 295-344.

[17] P.M. Harrison, F.A. Fischbach, and T. G, Hoy, etc. Nature. **1967**, 1180-1190.

[18] K.M. Towe. J. Biol. Chem. **1981**, 256, 9377-9388.

[19] X. Yang, Y. Chen-Barrett, P. Arosio, N.D. Chasteen. Biochemistry. **1998**, 37, 9743.

[20] John L. Jambor, John E. Dutrizac. Chem. Rev. **1998**, 98, 2549-2585.

[21] K. M. Towe, W. F Bradley. J. Colloid Interface Sci. **1967**, 24, 384.

[22] U. Schwertmann, R. M. Cornell. Iron Oxides in The Laboratory. VCH: New York, **1991**.

[23] R. A. Eggleton, R. W. Fitzpatrick. Clays Clay Miner. **1988**, 36,111.

[24] S. Hilty , B. Webb, R. B. Frankel, G. D. Watt. J. Inorg. Biochem. **1994**, 56(3), 173-185.

[25] D.D. Awschalom, J. F. Smyth, G. Grinstein, etc. Phys. Rev. Let. **1992**, 68(20), 3092-3095.

[26] J. Tejada, X. X. Zhang, etc. Phys. Rev. Let. **1997**, 79(9), 1754-1757.

[27] J. G. E. Harris, J. E. Grimaldi, and D. D. Awschalom. Phys. Rev. B. **1999**, 60(5), 3453-3456.

[28] Mamiya H, Nakatani I, Furubayashi T. Supperlattices and Microstructures. **2002**, 32(4-6), 179-186.

[29] Donald C. Zapien, Michael A. Johnson. J. Electroanalytical Chem. **2000**, 494, 114-120.

[30] Todd D. Martin, Scott A. Monheit, etc. J. Electroanalytical Chem. **1977**, 420, 279-290.

[31] Sasabe H, Furuno T, Otomo J, Tomioka H, Urabe Y, Nagamune T, Kim KH, Kobayashi K, Kobayashi Y. Thin Solid Films. **1992**, 216(1), 99-104.

[32] Frank Caruso, D. Neil Furlong, Peter Kingshot. J. Colloid and Interface Sci. **1997**, 186, 129-140.

[33] Li YM, Kim W, Zhang YG, Rolandi M, Wang DW, Dai HJ. J. Phys. Chem. **2001**, B, 105 (46), 11424-11431.

[34] Zhang Y, Li Y, Kim W, Wang D, Dai H. App. Phys. A-Materirals Science & Processing. **2002**, 74 (3), 325-328.

[35] Tominaga M, Ohira A, Kubo A, Taniguchi I, Kunitake M. Chem. Communications. **2004**, 1518-1519.

[36] Yamashita I. Thin Solid Films. **2001**,393(1-2), 12-18.

[37] J.M. Bonard, P. Chauvin, and C. Klinke. Nao Letters. **2002**, 2(6), 665-667.

[38] T. Douglas, V. T. Stark. Inorg. Chem. **2000**, 39, 1828-1830.

[39] P. Mackle, J. M. Charnock, C. D. Garner, F. C. Meldrum, S. Mann. J. Am. Chem. Soc. **1993**, 115, 8471-8472.

[40] F. C. Meldrum, T. Douglas, S. Levi, P. Arosio, S. J. Mann. J. Inorg. Bichem. **1995**, 58(1), 59-68.

[41] F. C. Meldrum, B.R. Heywood, S. Mann. Science. 1992, 257, 522-523.

[42] M. Okuda, K. Iwahori, I. Yamashita, H. Yoshimura. Biotech. Bioeng. **2003**, 84 (2), 187-194.

[43] Wong, K, K. W., Mann. S. Adv. Mater. **1996**, 8, 928-&.

[44] Gerald D. Watt. Analytical Biochemistry. **1979**, 99, 399-407.

[45] Watt FG, Frankel RB, Papaefthymiou GC. Proc. Natl. Acad. Sci. USA. **1985**, Jun, 82 (11), 3640-3.

[46] R.K. Watt, R.B Frankel and G. D. Watt. Biochemistry. **1992**, 31(40), 9673-9679.

[47] Jiwoong Park, Abhay Pasupathy, etc. Nature. **2002**, 417, 722-725.

[48] David L. Klein, Richard Roth, etc. Nature. **1997** , 389, 699-701.

[49] J. Junno, S.B. Carlsson, etc. App. Phys. Let. **1998**, 72(5), 548-550.

[50] Xiaoyin Xiao, Bingqian Xu, and Nongjian J. Tao. **2004**, 4(2), 267-271.

[51] Tanaka I, Kawasaki E, etc. Surface Science. **2003**, 801-805.

[52] Yoshitaka Okada, Masashi Miyagi, etc. J. App. Phys. **2001**, 90(1), 192-196.

[53] X. D. Cui, A, Primak, X. Zarate, etc. Nature. **2001**, 294, 571-574.

[54] Martin Hegner, Peter Wagner and Giorgio Semenza, Surface Sci. **1993**, 291, 39-46.

[55] H.W. Morrow and Robert P. Kokernak. Statics and Strength of Materials. Fifth Edition. Pearson Prentice Hall. **2004**, 737.

[56] William R. Smythe. Static and Dynamic Electricity. McGraw-Hill Book Company. Chapter V. 1950.

[57] B.L. Sharma. Metal-Semiconductor Schottky Barrier Junctions and Their Applications. Plenum Press: New York and London. **1984**.

[58] Physics of Semiconductor Devices. 2nd Edition. S.M. Sze. John Willey & Sons. **1981**.

[59] R.H. Good, Jr. and E.W. Muller. Handbuch der Physik (Springer-Verlag, Berlin, **1956**), Vol. XXI, 176.

[60] M. Lenzlinger and E. H. Snow. J. App. Phys. **1969,** 40(1), 278-282.

[61] Y. Miyamoto, A. Yamaguchi, etc. J. Vac. Sci. Technol. **1998**, B 16(2), 851-854.

[62] Alexander Olbrich, Bernd Ebersberger, and Christian Boit. App. Phys. Let. **1998**, 73(21), 3114-3116.

[63] S. J. O'Shea, R. M. Atta, M. P. Murrell, and M. E. Welland. J. Vac. Sci. Technol. **1995**, B 13(5), 1945-1952.

[64] J.G. Simmons. J. Phys. D: Appl. Phys. **1971**, 4, 613-657.

[65] John G. Simmons. J. Appl. Phys. **1963**, 34(6), 1793-1803.

Appendix 1. Twenty Amino Acids Used for Assembling Proteins

Amino acids contain both a carboxyl group (COOH) and an amino group (NH_2). The general formula for an amino acid is NH_2-CHR-COOH, where R indicate a side chain. Although the neutrally-charged structure is commonly written, it is inaccurate because the acidic COOH and basic NH_2 groups react with one another to form an internal salt called a zwitterion. The zwitterion has no net charge; there is one positive (COO^-) and one negative (NH_3^+) charge. So under normal cellular condition, the amino acid has both a positive and a negative charge, indicated as NH_3^+-CHR-COO^-. The following table shows amino acid names, three- and one-letter standard abbreviations, and linear structures (atoms in red are bonded to each other). Figure A1-1 shows the structures of 20 amino acids.

Name	Abbreviation	Linear Structure
Alanine	**ala** A	CH3-CH(NH2)-COOH
Arginine	**arg** R	HN=C(NH2)-NH-(CH2)3-CH(NH2)-COOH
Asparagine	**asn** N	H2N-CO-CH2-CH(NH2)-COOH
Aspartic Acid	**asp** D	HOOC-CH2-CH(NH2)-COOH
Cysteine	**cys** C	HS-CH2-CH(NH2)-COOH
Glutamic Acid	**glu** E	HOOC-(CH2)2-CH(NH2)-COOH
Glutamine	**gln** Q	H2N-CO-(CH2)2-CH(NH2)-COOH
Glycine	**gly** G	NH2-CH2-COOH
Histidine	**his** H	NH-CH=N-CH=C-CH2-CH(NH2)-COOH
Isoleucine	**ile** I	CH3-CH2-CH(CH3)-CH(NH2)-COOH
Leucine	**leu** L	(CH3)2-CH-CH2-CH(NH2)-COOH
Lysine	**lys** K	H2N-(CH2)4-CH(NH2)-COOH
Methionine	**met** M	CH3-S-(CH2)2-CH(NH2)-COOH
Phenylalanine	**phe** F	Ph-CH2-CH(NH2)-COOH

Proline	**pro** P	NH-(CH2)3-CH-COOH
Serine	**ser** S	HO-CH2-CH(NH2)-COOH
Threonine	**thr** T	CH3-CH(OH)-CH(NH2)-COOH
Tryptophan	**trp** W	Ph-NH-CH=C-CH2-CH(NH2)-COOH
Tyrosine	**tyr** Y	HO-Ph-CH2-CH(NH2)-COOH
Valine	**val** V	(CH3)2-CH-CH(NH2)-COOH

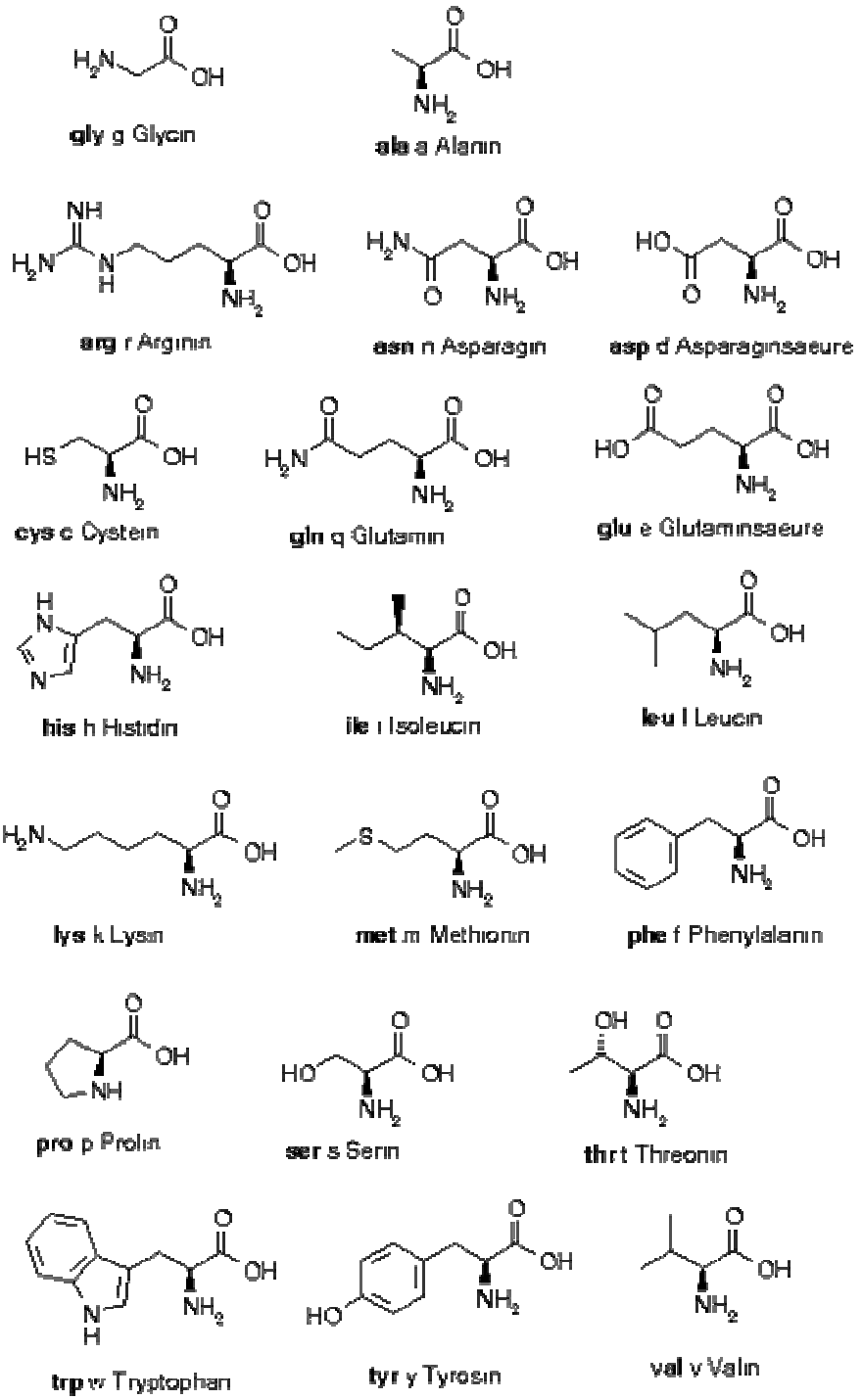

Figure A1-1. The structures of 20 amino acids.

Appendix 2. Tapping Mode AFM Images of Ferritin Molecules on Flat Gold Surfaces

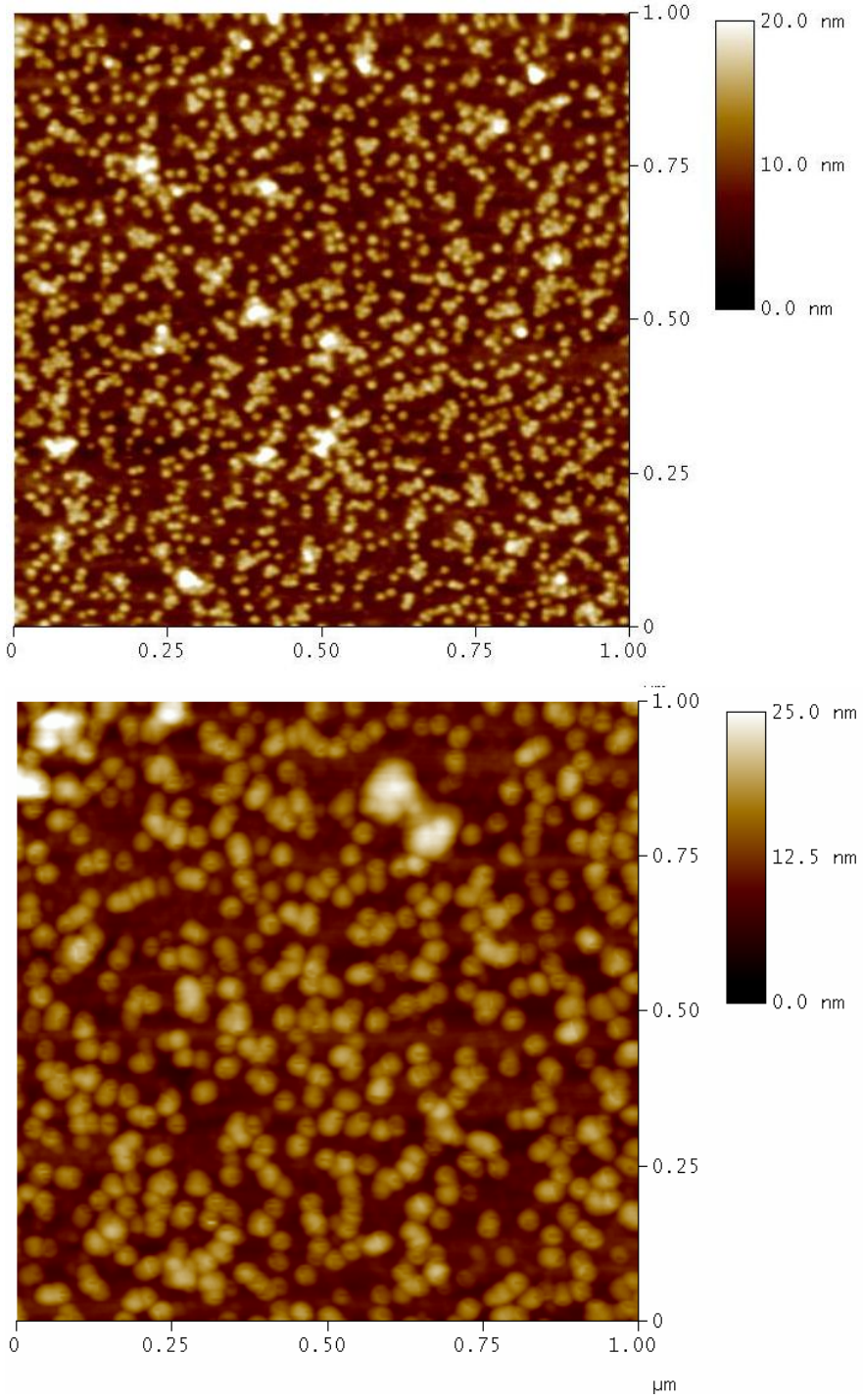

Figure A2-1. Apo HoSF tapping mode AFM images

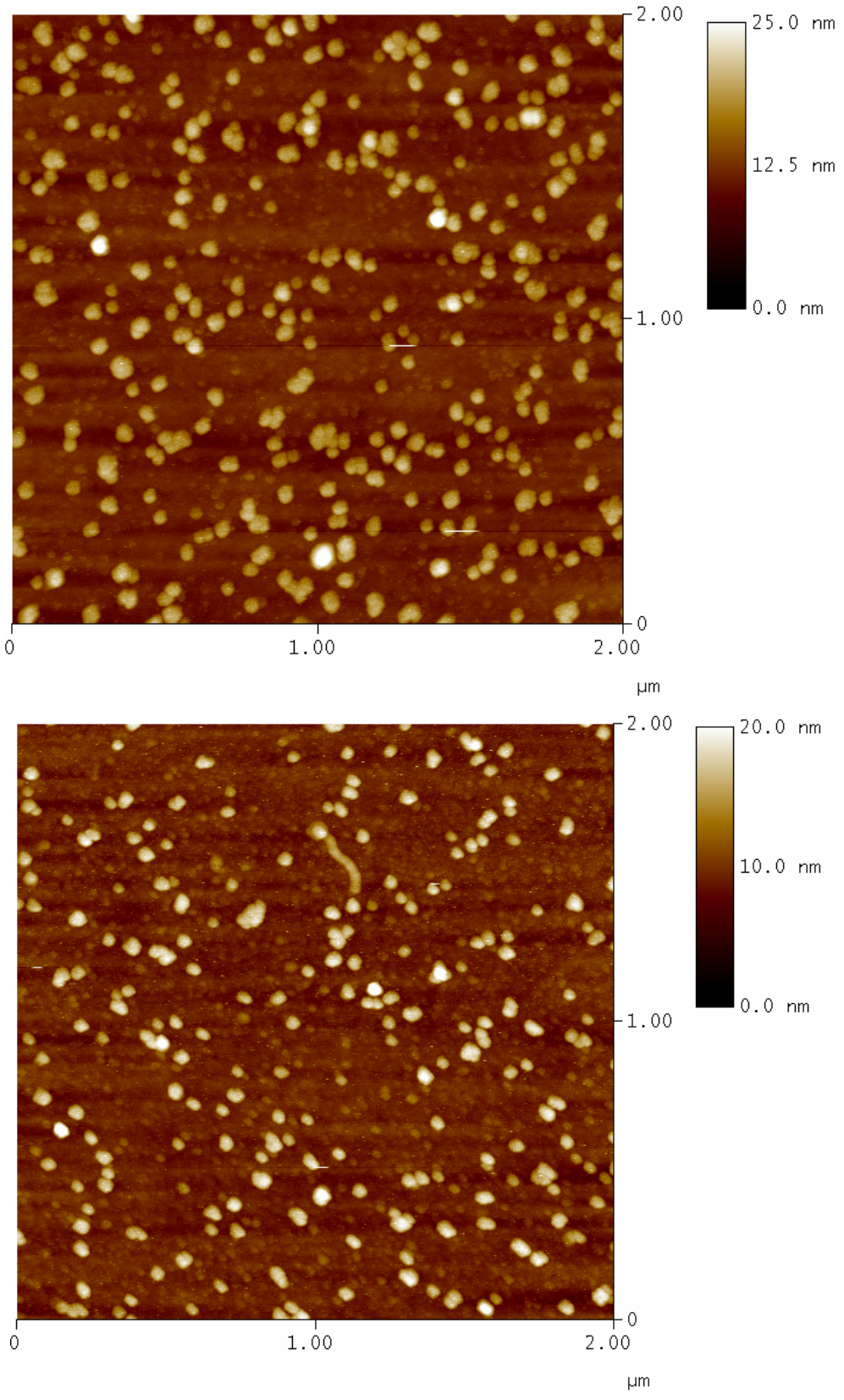

Figure A2-2. Holo HoSF tapping mode AFM images

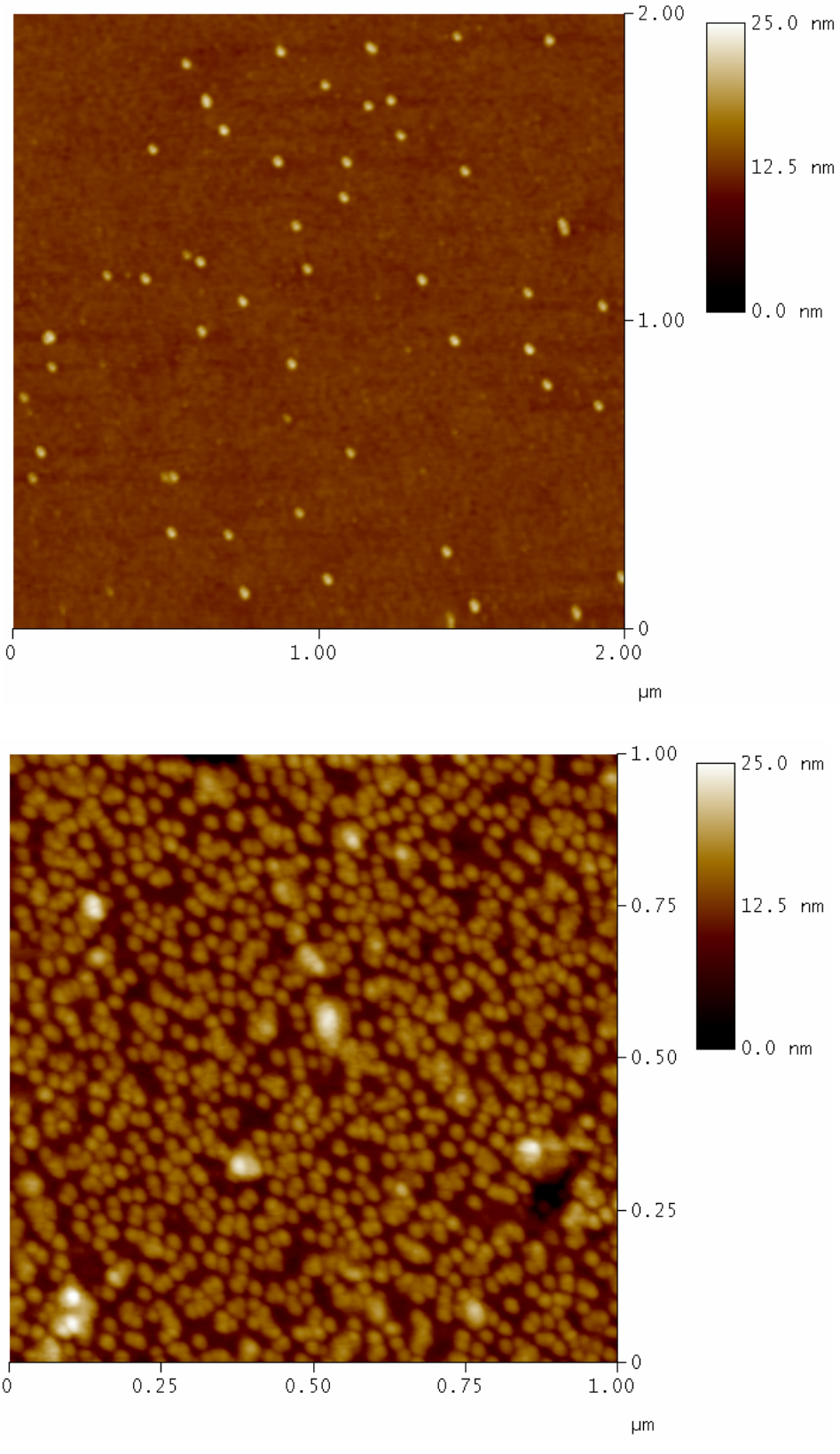

Figure A2-3. Holo AvBF tapping mode AFM images.

Appendix 3. The Nanocript Programs and Labview Programs for Single Ferritin AFM Conductivity Measurements

The following C program (Nanoscript Program 1, version 4.43r8) is used to move the AFM tip down, trigger the Labview programs (version 6.1) to do the I-V measurements and send the depth of the tip to the Labview programs. The corresponding Labview program used to do the I-V measurements are shown in Figure A3-1 and Figure A3-2. Another C program (Nanoscript Program 2) is used to move the AFM tip down slowly (step by step) and move the tip up slowly so that it can trigger another Labview program to do the tip deflection-depth measurement and the current-depth measurement at the same time. The corresponding Labview program used to do the deflection-depth and the current-depth measurements are shown in Figure A3-3 and Figure A3-4.

```
********************     Nanoscript Program 1     **********************

//Degao Xu
//Created Otc,10,2002

#include<litho.h>
void main()
{
      LITHO_BEGIN
      LithoDisplayStatusBox();      //display litho status box
      LithoScan(FALSE);              //turn off scanning
      LithoCenterXY();               //move the tip to center of feild

      double depth = 0.06;           //move the tip 60nm down
      double pause_time = 32.0;    //pause for some fixed time
      double z_rate = 0.020 ;        //move the dip down at 20nm/s

      LithoMoveZ(-1*depth, z_rate);
      LithoSet(lsAna2,2+depth*10);
      LithoPause(pause_time);
      LithoSet(lsAna2, 0);
      LithoMoveZ(depth, z_rate);

      LithoRemoveStatusBox();
      LITHO_END
}
********************     End of Nanoscript Program 1 **********************
```

```
********************     Nanoscript Program 2 ********************
//Degao Xu
//Created June 29,2004

#include<litho.h>
void main()
{
      LITHO_BEGIN
      LithoDisplayStatusBox();                  //display litho status box
      LithoScan(FALSE);                         //turn off scanning
      LithoCenterXY();                          //move the tip to center of feild

      double depth = 0.08;                      //move the tip 80nm down (unit: um)
      double initial_depth = 0.040;             //Tip moves to this depth first
      double pause_time = 0.0005;               //pause for some fixed time
      double z_rate = 0.040 ;                   //move the dip down at 40nm/s
      double temp_depth=initial_depth;          //Tip moves to this depth first
      double step_size=0.0005;                  //step_size: 0.5nm

      LithoMoveZ(-1*temp_depth, z_rate);

      //tip push down
      while(temp_depth<=depth)
      {
            LithoSet(lsAna2,2+temp_depth*10);
            LithoPause(pause_time);
            LithoMoveZ(-1*step_size, z_rate);
            temp_depth=temp_depth+step_size;
      }
      //Tip withdraw
      while(temp_depth>=initial_depth)
      {
            LithoMoveZ(step_size, z_rate);
            temp_depth=temp_depth-step_size;
            LithoSet(lsAna2,2+temp_depth*10);
            LithoPause(pause_time);
       }

      LithoSet(lsAna2, 0);
      LithoMoveZ(temp_depth, z_rate);
      LithoRemoveStatusBox();
      LITHO_END
}
********************     End of Nanoscript Program 2 ********************
```

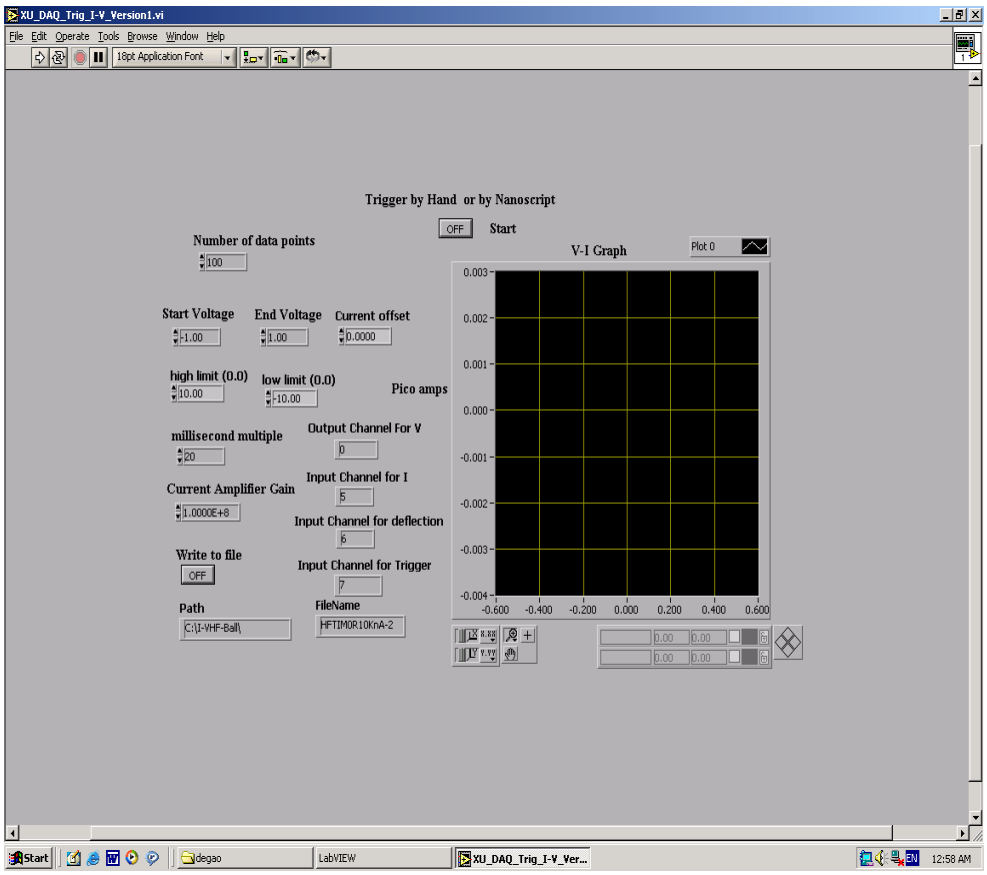

Figure A3-1. The panel of the Labview program for the I-V measurements.

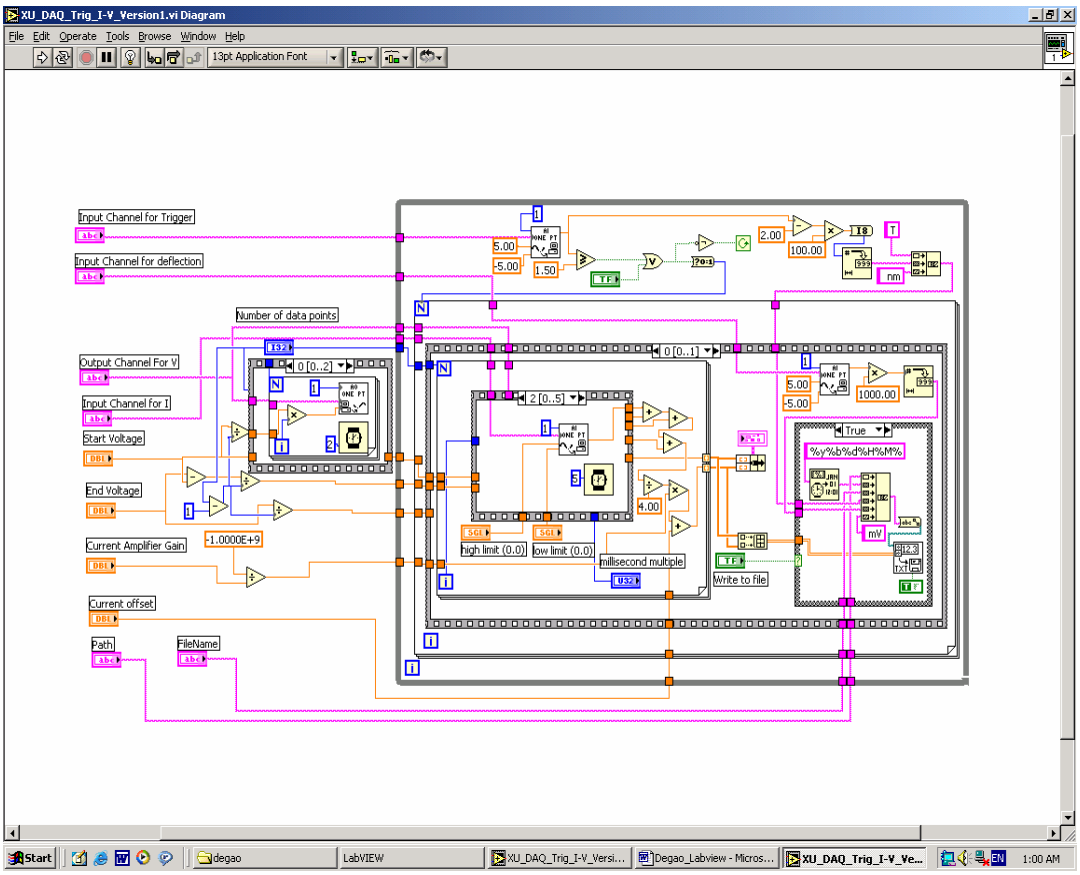

Figure A3-2. The diagram of the Labview program for the I-V measurements.

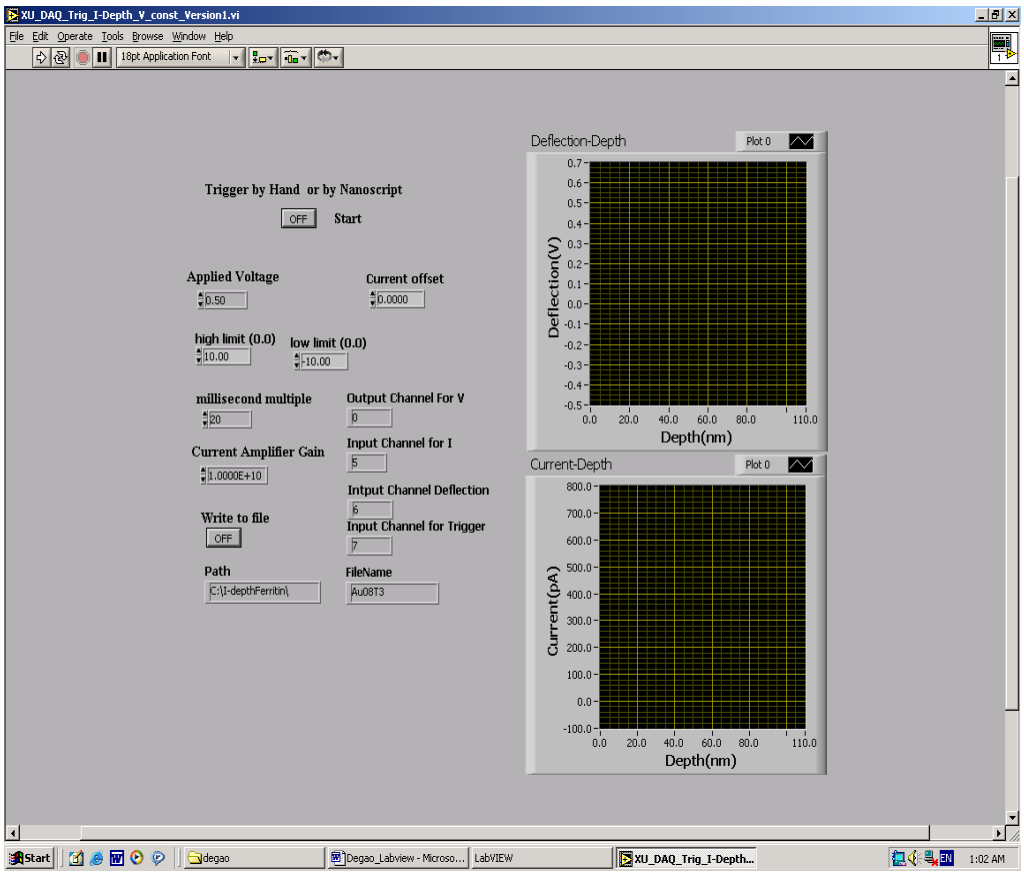

Figure A3-3. The panel of the Labview program for the deflection-depth and current-depth measurements.

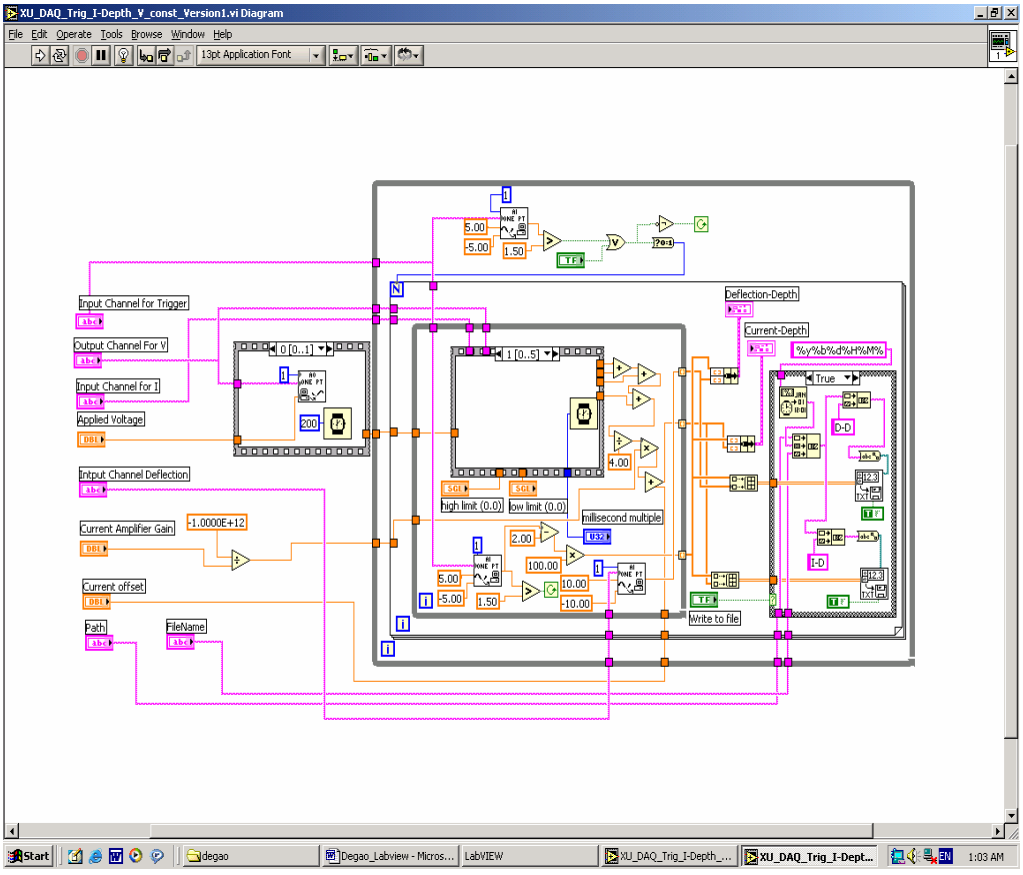

Figure A3-4. The diagram of the Labview program for the deflection-depth and current-depth measurements.

Appendix 4. The Relationship between the AFM Tip Size and the Lateral Image Size of Ferritin Molecules

The lateral size of the image of a ferritin will be significantly larger than the ferritin size if the tip size is comparable to or even larger than the ferritin size. We can roughly estimate their relationship. We assume the end of the AFM tip has a spherical shape with a radius R_1, and the ferritin molecule, which is fixed on a flat surface, is a hard ball with a radius R_2. We can build XY coordinates (X axis is on the flat surface and Y axis passes through the center of ferritin molecule) as shown in Figure A4-1. If we assume $R_1 \geq R_2$, then while the tip touches the ferritin, the very top point of the tip with coordinate (x, y) will follow a path (shown as dark thick curve in Figure A4-1) which can be described as:

$$x^2+(y+R_1-R_2)^2 = (R_1+R_2)^2.$$

The radius R of the ferritin image satisfies the following equation:

$$R^2+(R_1-R_2)^2=(R_1+R_2)^2.$$

So $R=2(R_1*R_2)^{1/2}$. Therefore, the image of the ferritin should have height $2R_2$ and lateral diameter $D=4(R_1*R_2)^{1/2}$. So from the image of a ferritin molecule, we can find the height of the ferritin under AFM tip, and we can also estimate the size of the tip by the equation $R_1 = D^2/16R_2 = D^2/8h$, where h is height of the image of the ferritin molecule.

If the AFM tip is so sharp that the radius of the curvature of a tip is much smaller than the size of the ferritin molecule, then the image shape of a ferritin molecule may be a little different as shown in Figure A4-2. The top part of the image

is close to the trace of a circle while the two sides of the image are close to straight lines. The lateral radius of the image R is close to $R_2 \tan(45°+\phi/4)$, where ϕ is the cone angle of the tip. So the image of a ferritin molecule has a height $2R_2$ and lateral diameter $D = 2R_2 \tan(45°+\phi/4)$.

Figure A4-3 shows the image of a single bacteria holoferritin and its cross section. The height of image is 9.7nm and the lateral diameter of image is 60nm. So the estimated tip radius is ~45nm.

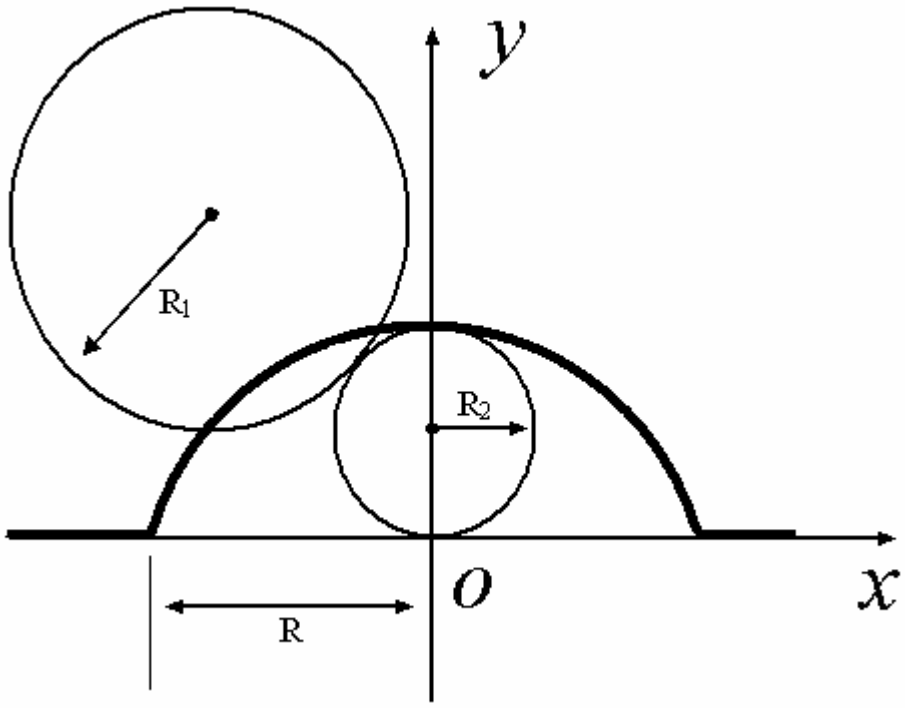

Figure A4-1. The relationship among the size of the image of a ferritin molecule and the sizes of the tip and ferritin when the tip size is comparable to the ferritin size. R_1 is the radius of the tip. R_2 is the radius of a ferritin molecule. The path of the tip is shown by the thick curve with radius $R=2(R_1*R_{2)}^{1/2}$.

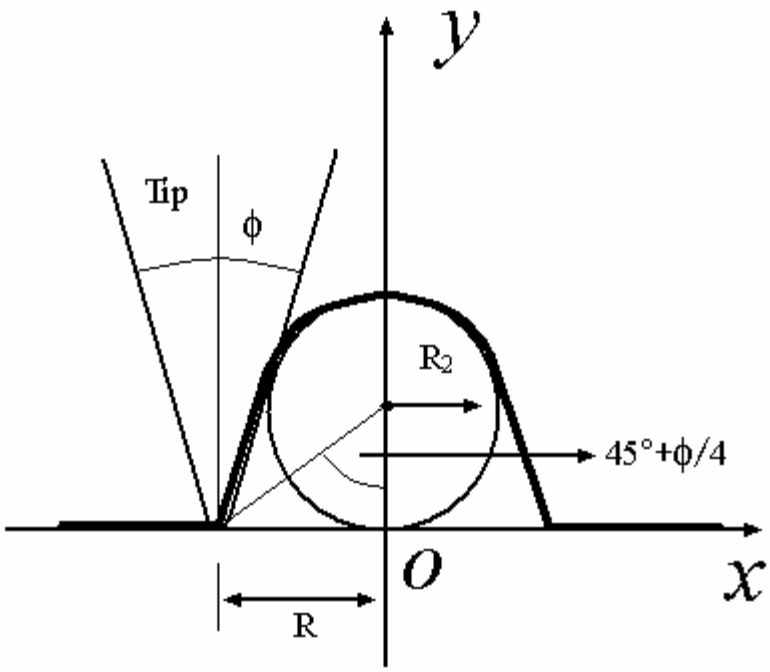

Figure A4-2. The relationship among the size of the image of a ferritin molecule and the sizes of the tip and ferritin when the tip size is much smaller than the ferritin size. ϕ is the cone angle of the tip. R_2 is the radius of a ferritin molecule. The path of the tip is shown with thick curve. The radius of the image R is about $R_2 \tan(45°+\phi/4)$.

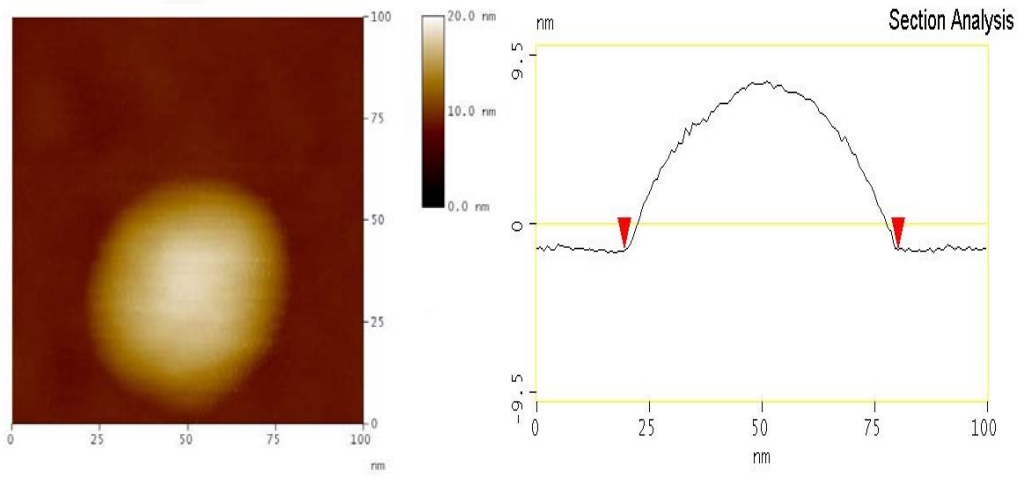

Figure A4-3. A tapping mode AFM image of a bacterial ferritin and its cross section. The height of the image is 9.7 nm and the lateral diameter is 60 nm.

Appendix 5. Electrical Field Distribution between the AFM Tip and Au Substrate and the Attractive Force between Them

First, just consider the case of two conductive spheres[56]. Assume there is a conductive sphere (sphere I) with radius a. It holds a potential V_1. Then the potential outside the sphere is:

$$V(r) = \frac{aV_1}{r} = \frac{q}{4\pi\varepsilon_0 r},$$

where $q = 4\pi\varepsilon_0 a V_1$. We can consider there is a charge q at the center of sphere I. Now put another conductive sphere (sphere II) with radius b near sphere I as shown in the Figure A5-1. Sphere II keeps a potential V=0. The distance between the two centers of spheres is c. Let m=a/c and n=b/c. The image charge of charge q in sphere II is:

$$q_1 = -qb/c = -nq$$

at a distance $d_1 = b^2/c = n^2 c$ to the left of the center of sphere II. This image generates another image charge:

$$q_2 = -q_1 a/(c - d_1) = mnq/(1 - n^2)$$

at a distance $d_2 = a^2/(c - d_1) = m^2 c/(1 - n^2)$ to the right of the center of sphere I. Another image charge is generated in sphere II:

$$q_3 = -q_2 b/(c - d_2) = -mn^2 q/(1 - m^2 - n^2)$$

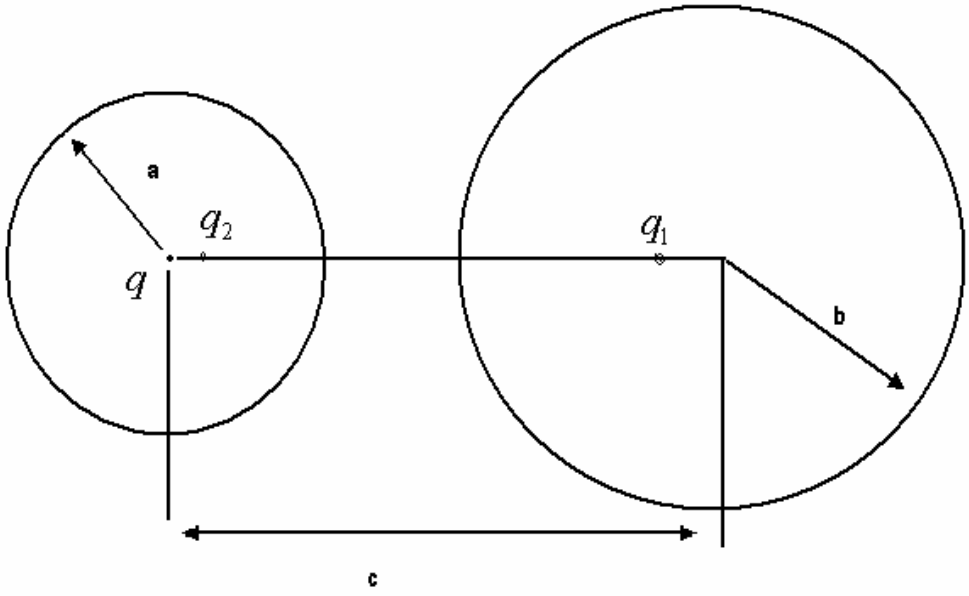

Figure A5-1. Two conductive spheres (sphere I and sphere II) with radius a and b respectively. Their separation is c. q1 is the image charge generation by the charge q holding by the conductive sphere I and q2 is the image charge generated by the charge q1.

at a distance $d_3 = b^2/(c-d_2) = n^2(1-n^2)c/(1-m^2-n^2)$ to the left of the center of sphere II. The forth image charge is:

$$q_4 = -q_3 a/(c-d_3) = m^2 n^2 q/((1-n^2)^2 - m^2)$$

at a distance $d_4 = a^2/(c-d_3) = m^2(1-m^2-n^2)c/((1-n^2)^2-m^2)$ to the right of the center of sphere I, and so forth.

Now the total charge in sphere I is:

$$Q_1 = q + q_2 + q_4 ... = q(1 + mn/(1-n^2) + m^2 n^2/((1-n^2)^2 - m^2) + ...) = V_0 c_{11}$$

and the total charge in sphere II is

$$Q_2 = q_1 + q_3 + ... = q(-n - mn^2/(1-m^2-n^2) - ...) = V_0 c_{12}$$

If the sphere II holds a potential V_2 and $q_2 = 4\pi\varepsilon_0 b V_2$, then

$$Q_1 = V_1 c_{11} + V_2 c_{21} \quad \text{and} \quad Q_2 = V_1 c_{12} + V_2 c_{22}$$

where

$$c_{11} = 4\pi\varepsilon_0 a(1 + mn/(1-n^2) + m^2 n^2/((1-n^2)^2 - m^2) + ...)$$

$$c_{11} = c_{21} = 4\pi\varepsilon_0 ab(-1 - mn/(1-m^2-n^2) - ...)/c$$

$$c_{22} = 4\pi\varepsilon_0 b(1 + mn/(1-m^2) + m^2 n^2/((1-m^2)^2 - n^2) + ...)$$

Now if we assume $V_2 = 0$ again, then the attraction force between the two spheres is:

$$F = \frac{V_1^2 \partial c_{11}}{2\partial c} = -\frac{4\pi\varepsilon_0 a V_1^2}{c}\{\frac{mn}{(1-n^2)^2} + \frac{m^2 n^2[2(1-n^2)+m^2]}{[(1-n)^2 - m^2]^2} + ...\}$$

From the above analysis, the surface electrical field of sphere I at the nearest point to the sphere II is:

$$E=\frac{q}{4\pi\varepsilon_0}\{\frac{1}{a^2}-\frac{n}{(c-n^2c-a)^2}+\frac{mn}{1-n^2}\frac{1}{(a-m^2c/(1-n^2))^2}$$
$$+\frac{mn^2}{(1-m^2-n^2)}\frac{1}{(c-n^2(1-n^2)c/(1-m^2-n^2)-a)^2}$$
$$+\frac{m^2n^2}{((1-n^2)^2-m^2)}\frac{1}{(a-m^2(1-m^2-n^2)c/((1-n^2)^2-m^2))^2}-....\}$$

or

$$E=\frac{V_1}{a}\{1+\frac{nm^2}{(1-n^2-m)^2}+\frac{mn}{1-n^2}\frac{1}{(1-m/(1-n^2))^2}$$
$$+\frac{mn^2}{(1-m^2-n^2)}\frac{m^2}{(1-n^2(1-n^2)/(1-m^2-n^2)-m)^2}$$
$$+\frac{m^4n^2}{((1-n^2)^2-m^2)}\frac{1}{(1-m(1-m^2-n^2)/((1-n^2)^2-m^2))^2}+....\}$$

Now consider our special case of a plane (namely $b\to\infty$) and a sphere with radius a. If d is the distance from plane surface to the center of the sphere, then d=c-b, $m\to 0$, $n\to 1$ and $m/(1-n)=a/d$. So we have

$$c_{11}=4\pi\varepsilon_0 a(1+\frac{a}{2d}+\frac{a^2}{4d^2-a^2}+...)$$

$$F=\frac{V_1^2\partial c_{11}}{2\partial d}=-2\pi\varepsilon_0 a^2V_1^2\{\frac{1}{2d^2}+\frac{8ad}{(4d^2-a^2)^2}...\}$$

The surface electrical field of sphere I at the nearest point to the plane is:

$$E=\frac{V_1}{a}\{1+\frac{a^2}{(2d-a)^2}+\frac{a}{2d}\frac{1}{(1-a/2d)^2}+\frac{a}{2d}+\frac{(2d-a)^2}{2d^2-a^2}....\}$$

Appendix 6. The C Program for Calculation of the Electric Field between the Conductive Tip and the Conductive Flat Surface

```
/* This code is used to calculate the electric
field at a conductive sphere(with radius a) surface
which holds a constant potential V1. The other conductive
sphere(with radius b) holds a constant potential V2=0.
The separation of the two closest surface is c.

This file was created in March 2004 by Degao Xu

Edited by nedit.
CC fielddata.c -o runfile
runfile >> data8nm.txt => append the result.
runfile > data8nm.txt => create a new file(delete the old file if it resists)
*/

#include <stdio.h>
#include <math.h>
#include <iostream.h>

int main()
{
    long double V1, q1, E_ave, Efield, E_high=0, E_low=0, q11, q12, d1,
                d2, a, b, c, step, s, V;
    int   i, j, N, points;

    V1 = 1.00;
    a  = 10e-9;
    //a  = 100;
    b  = 100;
    c  = 10e-9;
    N  = 30;
    points = 50;

    //============================================================
    q1= 4*3.14159265*8.8542e-12*a*V1;
    E_ave=V1/c;
    //printf("%0.4Lf%s%0.4Lf%s", q1,"\n", V1,"\n");
    cout.setf(ios::scientific,ios::floatfield);
    cout<<"Initial values: V1="<<V1<<"volts. a="<<a<<"m, b="<<b<<"m,
        c="<<c<<"m"<<endl;
    cout<<"The average electric field(V1/c):"<<E_ave<<endl;

    Efield=q1/(4*3.14159265*8.8542e-12*a*a);
    d2=0;
    q12=q1;
    cout<<endl<<"The calculated feild:"<<endl;
```

```
 cout<<"Initial field(V1/a): "<<Efield<<" The initial charge q1:
    "<<q1<<endl;

 cout<<"n   q11/q12       d1           E1           q12/q11
     d2          E2"<<endl;
for(i=1; i <= N; i++)
{
   q11 = -q12*b/(a+b+c-d2);
   d1  = b*b/(a+b+c-d2);
   Efield +=-q11/(4*3.14159265*8.8542e-12*(c+b-d1)*(c+b-d1));
   if(i<=10 || i==N)
      cout<<i<<"   "<<q11/q12<<"   "<<d1<<"   "<<Efield<<"   ";
   q12 = -q11*a/(a+b+c-d1);
   d2 = a*a/(a+b+c-d1);
   Efield +=q12/(4*3.14159265*8.8542e-12*(a-d2)*(a-d2));
   if(i<=10 || i==N)
     cout<<q12/q11<<"   "<<d2<<"   "<<Efield<<endl;
}
cout<<"Ratio of E_cal and E_ave: "<<Efield/E_ave<<"    Done!!"<<endl;

step=c/points;
cout<<"s             E             V"<<endl;
for(j=0; j<=points; j++)
{
   s=j*step;
   Efield=q1/(4*3.14159265*8.8542e-12*(a+s)*(a+s));
   V=q1/(4*3.14159265*8.8542e-12*(a+s));
   d2=0;
   q12=q1;
   for(i=1; i <= N; i++)
   {
     q11 = -q12*b/(a+b+c-d2);
     d1  = b*b/(a+b+c-d2);
    Efiel+=-q11/(4*3.14159265*8.8542e-12*(c+b-d1-s)*(c+b-d1-s));
     V += q11/(4*3.14159265*8.8542e-12*(c+b-d1-s));
     q12 = -q11*a/(a+b+c-d1);
     d2 = a*a/(a+b+c-d1);
     Efield +=q12/(4*3.14159265*8.8542e-12*(a-d2+s)*(a-d2+s));
     V +=q12/(4*3.14159265*8.8542e-12*(a-d2+s));
   }
   if(j==0) E_high=Efield;
   if(j==points) E_low=Efield;
   cout<<s<<"   "<<Efield<<"   "<<V<<endl;
}
cout<<"E_high/E_ave: "<< E_high/E_ave <<" E_ave/E_low: "<<
E_ave/E_low <<endl;
return 0;
}
```

Appendix 7. The Effect of Image Charge for Fowler Nordheim Tunneling

If the image charge of the tunneling electron is considered, then the potential barrier is[58]:

$$V(x) = C - qEx - \frac{q^2}{16\pi\varepsilon_r\varepsilon_0 x}$$

for x>0. The maximum potential energy is at the position

$$x_m = \sqrt{\frac{q}{16\pi\varepsilon_r\varepsilon_0 E}}$$

The actual barrier height is lowered by:

$$\Delta\phi_B = \sqrt{\frac{qE}{4\pi\varepsilon_r\varepsilon_0}}$$

For our experiments, the maximum electric field is about 3V/10nm. If we assume ε_r=10, then

$\Delta\phi_B$=0.21eV

After considering the image charge, two new functions are introduced into the FN Equation[59]:

$$I(E) = \frac{A_{eff} q^3 E^2 m^*}{8\pi h\Phi_B m t^2(\frac{\sqrt{q^3E}}{\Phi_B})} \exp\left[\frac{-8\pi\sqrt{2m^*}\Phi_B^{3/2}}{3hqE} v(\frac{\sqrt{q^3E}}{\Phi_B})\right]$$

where

$$v(y) = [1 + (1 - y^2)^{1/2}]^{1/2} \{P(y) - (1 - [1 - y^2)^{1/2}]^{1/2} Q(y)\} / 2^{1/2}$$

$$P(y) = \int_0^{\pi/2} [1 - \frac{2(1 - y^2)^{1/2}}{1 + (1 - y^2)^{1/2}} \sin^2 \alpha]^{1/2} d\alpha,$$

$$Q(y) = \int_0^{\pi/2} [1 - \frac{2(1 - y^2)^{1/2}}{1 + (1 - y^2)^{1/2}} \sin^2 \beta]^{-1/2} d\beta$$

$$t(y) = v(y) - \frac{2}{3} y \frac{dv(y)}{dy}$$

when y varies from 0 to 1, v(y) varies from 1 to 0 and t(y) varies from 1 to 1.1107. The behaviors of functions v(y) and t(y) are shown in Figure A7-1. For our experiments, the maximum electric is about 3V/10nm. If we assume Φ_B is 0.5eV, then $y = \frac{\sqrt{q^3 E}}{\Phi_B} = 1.4 \times 10^{-4}$, and both v(y) and t(y) are very close to 1. So we can neglect functions v(y) and t(y) in the FN equation. In section 5.3, we fitted the measured I-V curves of horse spleen ferritins to the FN tunneling current equation.

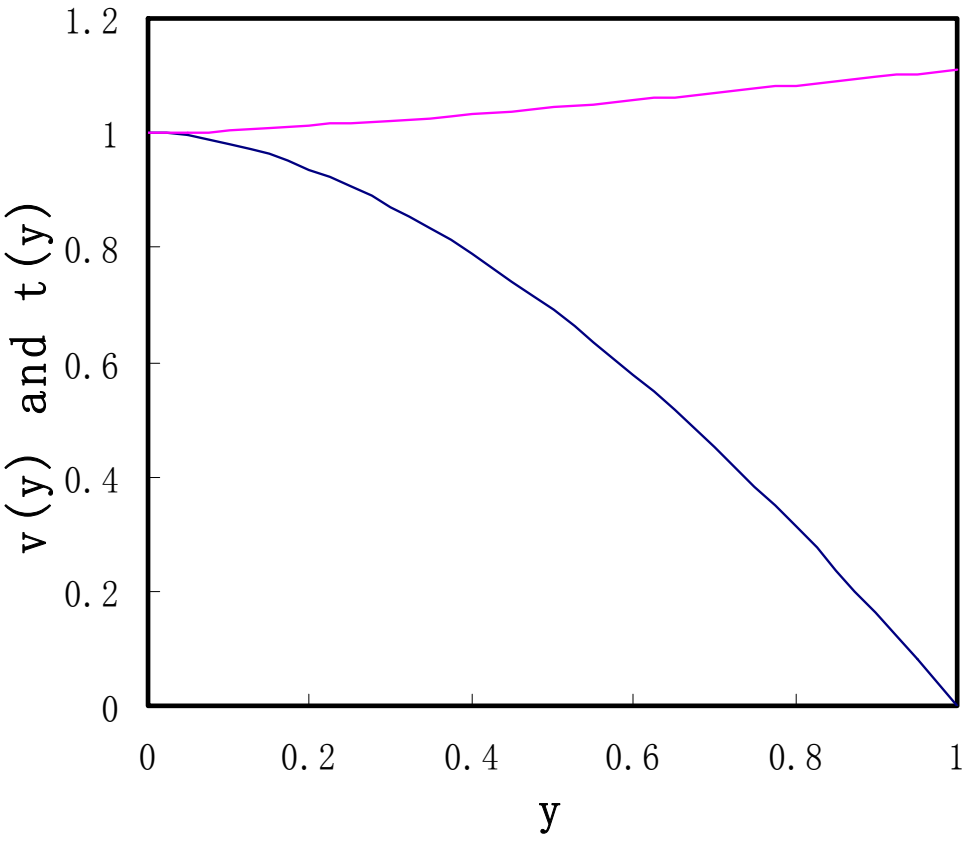

Figure A7-1. The functional forms of v(y) and t(y).

Appendix 8. Simmons Tunneling

For metal-insulator-metal junctions, a more general tunneling current is given by[64]:

$$J = 4\pi \frac{em}{h^3} \int_0^{\infty} dE(f_c(E) - f_a(E)) \int_0^{E} P(E_x) dE_x$$

where

$$f_c(E) = (1 + \exp(\frac{E - E_f}{kT}))^{-1}$$

and

$$f_a(E) = (1 + \exp(\frac{E + eV - E_f}{kT}))^{-1}$$

are the electron distribution in the cathode and anode electrodes respectively.; E_f is the Fermi energy of the cathode; V is the applied voltage between the cathode and anode; E and E_x are the energy and 'x-directed' energy of the electron respectively; and $P(E_x)$ is the electron tunneling probability through the insulator. By using the above equation, Simmons got a general current formula for electron tunneling through any arbitrary potential barrier[65] for metal-insulator-mental:

$$J = J_0 \{\bar{\phi} \exp(-A\bar{\phi}^{1/2}) - (\bar{\phi} + eV) \exp[-A(\bar{\phi} + eV)^{1/2}]\}$$

where

$$J_0 = e / 2\pi h(\beta \Delta s)^2$$
$$\bar{\phi} = \frac{1}{\Delta s}\int_{s_1}^{s_2} \phi(x)dx$$
$$\beta = 1 - \frac{1}{8\bar{\phi}^2 \Delta s}\int_{s_1}^{s_2} [\phi(x) - \bar{\phi}]^2 dx$$
$$A = (4\pi\beta\Delta s / h)(2m)^{1/2}$$

Parameters $\phi(x)$, s_1, s_2 are shown in Figure A8-1 and $\Delta s = s_2 - s_1$.

For a rectangular potential barrier with barrier height ϕ_B shown in Figure A8-2, we can get different tunneling equations in different voltage ranges. When V is close to 0 volt or $V << \phi_B/e$, J and V have a linear Relationship:

$$\Delta s = s,$$
$$\bar{\phi} = \phi_B,$$
$$\beta = 1,$$
$$J = CV,$$

where $C = \frac{3e(2m\phi_B)^{1/2}}{2sh}\exp[-\frac{4\pi s(2m\phi_B)^{1/2}}{h}]$. This linear equation can't be used to find the barrier height.

When $V < \phi_B/e$,

$$\Delta s = s,$$
$$\bar{\phi} = \phi_B - eV/2,$$
$$\beta \approx 1,$$
$$J = A\{(\phi_B - \frac{eV}{2})\exp[-B(\phi_B - \frac{eV}{2})] - (\phi_B + \frac{eV}{2})\exp[-B(\phi_B + \frac{eV}{2})]$$

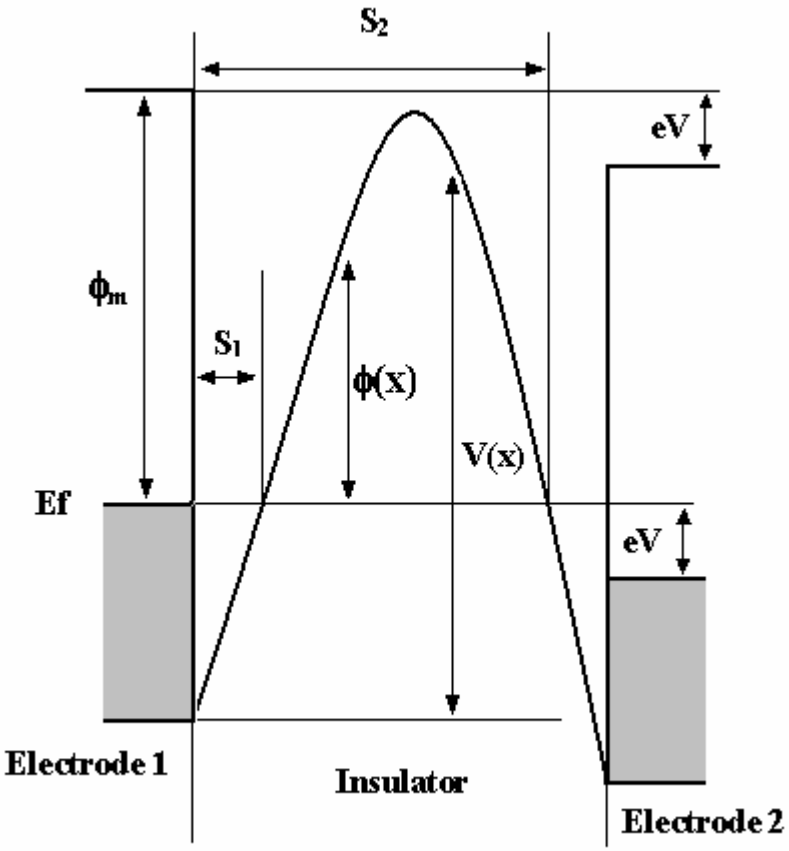

Figure A8-1. General potential barrier for a metal-insulator-metal junction. Φ_m is the work function of the metal. Ef is the Fermi energy of the metal. V is the applied voltage on the junction. V(x) is the potential barrier inside the insulator. $\Phi(x)$ is the potential barrier above the Fermi level. s_1 and s_2 are the limits of barrier at Fermi level.

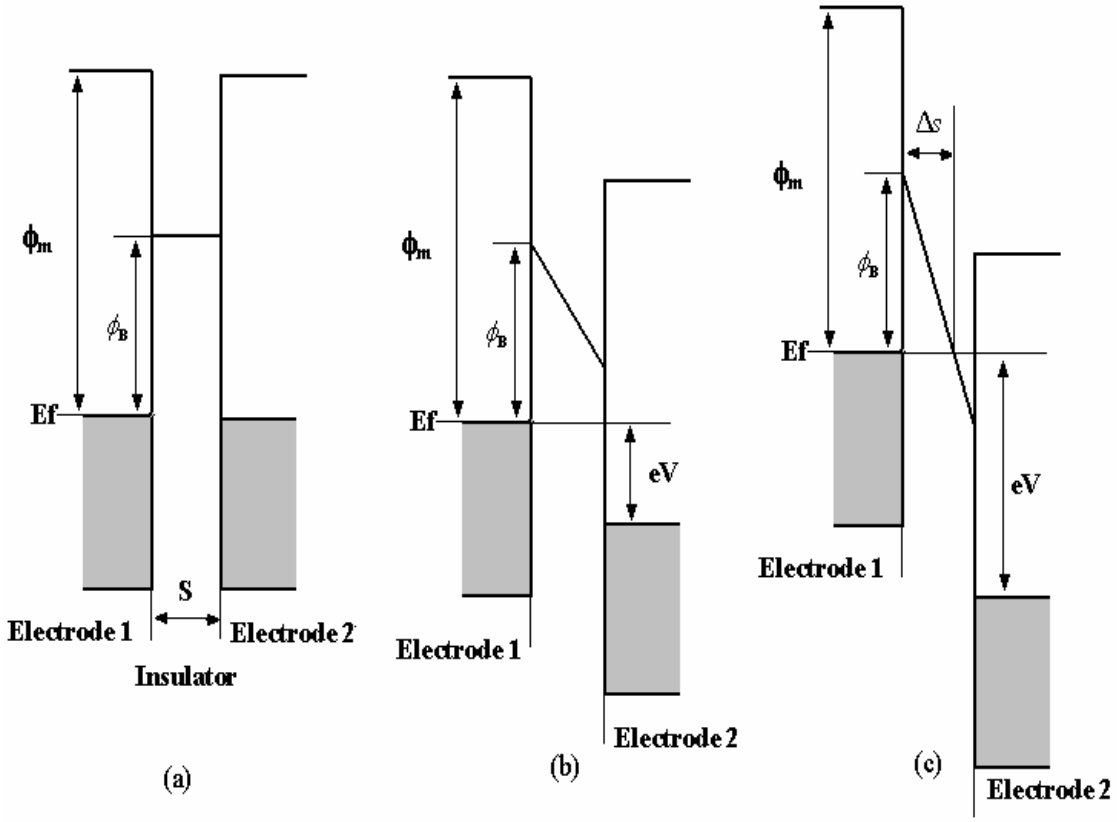

Figure A8-2. Rectangular potential barrier in a metal-insulator junction. (a) $V<<\phi_B/e$; (b) $V<\phi_B/e$; (c) $V>\phi_B/e$. V is the applied voltage to the junction. Ef is the Fermi energy of the metal. ϕ_B is barrier height between the metal and the insulator. S is the separation distance of the two electrode.

where

$$A = \frac{e}{2\pi h s^2},$$
$$B = \frac{4\pi s (2m)^{1/2}}{h}$$

When $V > \phi_B/e$,

$$\Delta s = s\phi_B / eV,$$
$$\bar{\phi} = \phi_B / 2,$$
$$\beta = 23/24,$$
$$J = AV^2\{\exp(-\frac{B}{V}) - (1+\frac{2eV}{\phi_B})\exp[-\frac{B}{V}(1+\frac{2eV}{\phi_B})]\}$$

where

$$A = \frac{2.2e^2}{8\pi h \phi_B s^2}$$
$$B = \frac{8\pi s (2m)^{1/2} \phi_B^{3/2}}{2.96he}$$

When $V > (\phi_B + E_f)/e$,

$$J = AV^2 \exp(-\frac{B}{V})$$

where

$$A = \frac{2.2e^2}{8\pi h \phi_B s^2}$$
$$B = \frac{8\pi s (2m)^{1/2} \phi_B^{3/2}}{2.96he}$$

This current equation is quite similar to the FN equation except the difference of two constant factors. These differences arise because of the variation of Δs below the Fermi level.

In the above discussions, the image charges of the tunneling electron is not considered. The image potential energy is:

$$V_i(x) = -\frac{q^2}{4\pi\varepsilon_r\varepsilon_0}[\frac{1}{2x} + \sum_{n=1}^{\infty}(\frac{ns}{n^2s^2 - x^2} - \frac{1}{ns})]$$

A good approximation of this equation is given by:

$$V_i(x) = -\frac{1.15\lambda s^2}{x(s-x)}$$

where

$$\lambda = \frac{e^2 \ln 2}{8\pi\varepsilon_r\varepsilon_0 s}.$$

Now if the image potential energy is taken to account then,

$$\phi(x) = \Phi_B - \frac{qVx}{s} - \frac{1.15\lambda s^2}{x(s-x)}.$$

By solving the equations $\frac{d\phi(x)}{dx} = 0$ to get s_1 and s_2, we get get:

$$\bar{\phi} = \frac{1}{\Delta s}\int_{s_1}^{s_2}\phi(x)dx = \phi_B - \frac{eV(s_1+s_2)}{2s} - \frac{1.15\lambda s}{s_2 - s_1}\ln\frac{s_2(s-s_1)}{s_1(s-s_2)}$$

For V<ϕ_B/e

$$s_1 = \frac{1.2\lambda s}{\phi_B}$$

$$s_2 = s(1 - \frac{9.2\lambda}{3\phi_B + 4\lambda - 2eV}) + s_1$$

For V> ϕ_B /e,

$$s_1 = \frac{1.2\lambda s}{\phi_B}$$

$$s_2 = \frac{(\phi_B - 5.6\lambda)s}{eV}$$